Liquid Crystals
Publication details, including instructions for authors and subscription information:
http://www.informaworld.com/smpp/title~content=t713926090

Liquid crystals: a chemical physicist's view

Geoffrey R. Luckhurst[a]
[a] School of Chemistry, University of Southampton, Southampton SO17 1BJ, United Kingdom

To cite this Article Luckhurst, Geoffrey R.(2005) 'Liquid crystals: a chemical physicist's view', Liquid Crystals, 32: 11, 1335 — 1364
To link to this Article: DOI: 10.1080/02678290500423128
URL: http://dx.doi.org/10.1080/02678290500423128

Liquid Crystals, Vol. 32, No. 11–12, November–December 2005, 1335–1364

Liquid crystals: a chemical physicist's view

GEOFFREY R. LUCKHURST
School of Chemistry, University of Southampton, Highfield, Southampton SO17 1BJ, United Kingdom

(*Received 6 September 2005; accepted 12 October 2005*)

This paper has allowed me the rare opportunity and pleasure of acknowledging those who have played important roles in my scientific career. It has also enabled me to report work in the field of liquid crystals which has gone unpublished. The particular topics have been selected because they illustrate the areas of liquid crystal science with which I have been especially concerned. The predicted phase diagram of mixtures of rods and spheres is both intricate and interesting. The ability to test these predictions experimentally has required the use of quasi-spherical solutes such as tetraethyltin. The reasons for the failure of the experiments to conform to theory are investigated and explained in terms of the orientational order of this flexible molecule, determined using deuterium NMR spectroscopy. The tetrapodes are more exotic tetrahedral structures in which four mesogenic groups are linked to a central atom or group. The massive flexibility of such molecules poses a severe problem for the prediction of their liquid crystal behaviour. Here a solution to this problem is presented and used to predict the dependence of the transitional properties of the tetrapodes on the spacer length and the mode of its attachment to the mesogenic group. The same molecular field approach has been employed to predict the variation of the transitional properties of liquid crystal dimers with the length of the spacer. It is found that for spacers containing about 12 or more atoms the odd–even effect predicted for the transitional properties varies significantly depending on the model used to describe the spacer conformation. That is, whether the torsional angles defining the conformations are taken to be discrete or continuous. Cyanobiphenyl dimers with spacers containing up to 24 atoms have been synthesized to test these predictions. The Gay–Berne potential has proved to be an important model with which to study liquid crystal behaviour using simulation techniques. By joining two Gay–Berne particles together with a flexible ethane link we have constructed a Gay–Berne dimer and have been able to explore the properties of this mesogen. In particular its phase behaviour, the novel structure of the smectic A phase and how the conformational distribution alters with the phase have been studied. Despite its attractive features there are relatively simple systems for which the Gay–Berne potential is not suitable. These include molecules with a spherocylindrical shape and those with a sphere embedded at the centre of such a structure. In fact the shapes of many mesogenic molecules approximate to the former, and certain metallomesogenic molecules have shapes like the latter. The novel Corner *S*-function potential provides a valuable way to represent such cylindrically symmetric shapes and we use this to simulate the behaviour of these systems. It is found that the sphere has a major influence on the phase behaviour as well as on the crystal structure.

1. Introduction

The Symposium held at Southampton to mark my 65th Birthday proved to be a wonderful occasion not only for me but, I believe, for all those present. The science presented and discussed was truly excellent and it was a special occasion at which to meet so many friends. I am really indebted to all of those who contributed to the success of the Symposium; to the participants and to the speakers as well as to the Organizing Group, George Attard, David Dunmur, Jim Emsley, Tim Sluckin and especially to Martin Bates who worked so hard and so effectively to make every aspect of this occasion just right. I also wish to add my thanks to the sponsors of the Meeting, Merck UK Ltd., Taylor & Francis Ltd. and Unilever Research (Port Sunlight); without their generous support the event would clearly not have been possible.

I have had the pleasure and privilege of helping to unravel some of the mysteries of liquid crystals for over 40 years. The vast majority of this time has been spent as a member of the Department now the School of Chemistry at the University of Southampton. This has provided a challenging, stimulating and supportive environment; I would not have wished to be anywhere else. My years at Southampton benefited immensely from a stream of able, talented and individual research students and postdoctoral fellows. It was a joy to have

Liquid Crystals
ISSN 0267-8292 print/ISSN 1366-5855 online © 2005 Taylor & Francis
http://www.tandf.co.uk/journals
DOI: 10.1080/02678290500423128

worked with them and has given me real pleasure and pride to see how their careers have developed. The award of Professorships both here and overseas to George Attard, Ian Hamley, Rauzah Hashim, Corrie Imrie, Claudio Zannoni and Habtamu Zewdie has been especially satisfying and rewarding. My research interests have been framed both by careful planning and by accident. These interests have been influenced by others and I want to acknowledge their formative contributions here.

My three years as an undergraduate at the University of Hull was especially pivotal. It was here that I first met George Gray whose stimulating and transparent lectures taught me much about organic chemistry. More importantly I learnt about the existence of the liquid crystal state of matter and its uniquely fascinating behaviour; this was to determine my research interests and continues to do so. I was privileged to study for my doctorate at Cambridge in the Department of Theoretical Chemistry headed by the inspirational Christopher Longuet-Higgins. He explained how important it was for theory to be guided by experiment and *vice versa*, which is the very essence of Chemical Physics. My primary research supervisor was Alan Carrington from whom I learnt much about the elegance of the quantum mechanics of magnetic resonance spectroscopy and the stimulation to be gained from ESR experiments. I hope that I also inherited from him some of his enthusiasm for scientific research; at the time it was certainly infectious. It was in Cambridge that Alan and I performed the first ESR experiment using a liquid crystal solvent. Our aim was to employ the ordering imposed by the liquid crystal to learn something about the structure of the free radical, which was the tetracyanoethylene anion. It was not until some years later that I was to invert the experiment and use ESR to investigate the behaviour of liquid crystals.

On graduation I decided that academia was not for me and, recently wed, left with my wife, Jan, for Zürich to take up a post in the Varian Research Laboratory as the ESR Applications Scientist. This resulted in a wonderful opportunity to work with the latest equipment and to interact with some of the best scientists. Amongst these was Warren Proctor who had been involved in the discovery of the chemical shift and who introduced me to solid state NMR spectroscopy. I then used this to measure a fairly rudimentary form of the proton NMR spectrum of PAA but this certainly impressed Alfred Saupe when he visited the Laboratory. It was also here that many of the ESR experiments involving liquid crystals were performed and my interests began to turn to the behaviour of the liquid crystal hosts. After two years in Zürich I thought again about academia and accepted an offer of a lectureship at Southampton. During the early days I was joined by Gian-Franco Pedulli and we worked with considerable success on the electron spin relaxation of systems containing more than one unpaired electron. The effects we observed were fascinating and our ability to explain them almost magical; this owes much to Franco's considerable insight. It was at Southampton that I met Jim Emsley who eventually persuaded me of the beauty of NMR spectroscopy and of its powerful potential for exploring the behaviour of liquid crystals. There then followed a wonderful period when we worked together on a wide variety of fascinating problems combining the power of molecular field theory and deuterium NMR spectroscopy. Outside of Southampton we worked with Neville Boden whose inquisitive attitude to science resulted in so many stimulating discussions. Bakir (Tim) Timimi joined us first as a sabbatical visitor and then on what proved to be an almost permanent basis. He is an extremely talented experimentalist and over the years has made our wild ideas reality. One of the most formative collaborations was with Pier-Luigi Nordio; this started in 1974 and continued until his untimely death in 1998. He was an inspirational friend who taught me much about theory, science, Italian culture, cuisine and life. At Southampton Tim Sluckin had joined the then Department of Mathematics and his interest in liquid crystals meant that we worked together on some challenging problems. What perhaps was more important was the unique benefit of hearing his views on almost any topic that was of concern to me. More recently a seemingly chance encounter with Akihiko Sugimura sensei in Southampton gave a quite new direction to my research interests. He introduced me to the importance of the macroscopic behaviour of nematics and together we have made some fascinating discoveries.

As I wrote this Introduction it soon became clear that I should not be able to mention all of those with whom I have interacted and who in one way or another helped to shape my interests in and attitude towards liquid crystals. I hope that they will forgive me for not mentioning them explicitly. My list of publications shows who they are and their contributions are certainly no less valued.

The support and understanding of my family has also played a major role in the way I have developed as a scientist. As a child my parents certainly indulged me by encouraging my interest and fascination in science, especially chemistry and mathematics, from my early days at School to the later years at University. Jan and

our wonderful daughters, Nicola and Caroline, have through their love ensured that I have been part of the real world. Without them I should have been far less of a person. Nicola and Caroline's charming husbands, Stephen and Mark, have certainly stimulated my interests in quite new areas and it is a joy to have them as members of a growing family. My fascination with liquid crystal science continues and I still delight in trying to unravel Nature's secrets, but now this is much tempered by the attention of our beautiful granddaughters, Clara and Minnie and by our recently arrived grandson, Samuel.

Much of my research has been published but there are, surprisingly, the results of certain projects that have not reached the open literature. They cover areas that I still consider to be exciting, important and certainly meriting publication. For these reasons I have decided to present some of them here. The selection I have made provides representative examples of my contributions to liquid crystal science; that is, in design and synthesis, experimental characterization using techniques such as ESR and NMR spectroscopy as well as neutron and X-ray scattering, molecular field theory and the computer simulation of model systems.

Five projects have been chosen and they are described in a way which gives the flavour of the project rather than providing the complete description expected for a full paper. In addition, I give the names of those who worked with me on the projects and in a very real sense they should be thought of as co-authors of that particular section of this paper. In the next section I deal with the novel phase behaviour predicted for a binary mixture of rods and spheres. The special interest here is the experimental studies designed to test these predictions and the failure of the theory to explain the behaviour of tetraethyltin dissolved in 4-pentyl-4′-cyanobiphenyl. NMR studies of perdeuteriated tetraethyltin show that this quasi-spherical molecule is in fact orientationally ordered in the nematic host. If allowance is made for this the observed phase behaviour proves to be in good accord with the modified theory.

Another fascinating class of molecules also has a tetrahedral core, these are the so-called tetrapodes in which four mesogenic groups are attached through flexible spacers to a central atom. This fascination stems from their surprising ability to form liquid crystalline phases. In §3 a molecular field theory capable of predicting the behaviour of these extremely flexible molecules is described. It is then employed to predict how the length of the alkyl chains and their mode of attachment to the mesogenic groups influence the nematic–isotropic transition temperature and the orientational order parameter of the mesogenic groups at this transition. These results suggest a range of intriguing tests of the theory for the tetrapodes. This was also found to be the case for liquid crystal dimers, which can be thought of as half a tetrapode. As we describe in §4, the theory predicts that the nematic behaviour of the dimers is strongly dependent on the model used to describe the conformations of the spacer linking the two mesogenic units. When the conformations are restricted to a discrete set the odd–even behaviour is especially marked, but when the spacer is able to adopt a continuous range of conformations the odd–even behaviour is rapidly attenuated. This difference is especially significant for long spacers and to test this prediction we have synthesized dimers with spacer lengths of up to 24 atoms.

The predictions are based on the molecular field approximation which is reliable at a semi-quantitative level but is certainly not quantitative. More reliable results are obtained from computer simulation studies and in §5 we describe a model developed for a liquid crystal dimer with a very short spacer linking two Gay–Berne molecules. The liquid crystal behaviour of this generic model has been simulated using molecular dynamics with inbuilt constraints. The model exhibits a nematic and a smectic A phase with a curious structure. The conformational distribution for the dimer is also of special interest because of the manner in which it changes with the phase. The shape of a Gay–Berne molecule is essentially ellipsoidal; this differs from that of real mesogenic molecules which approximates more to that of a spherocylinder. The Corner *S*-function potential is able to represent such a shape and can also be modified to provide a model potential for metallomesogens with large central groups. The nature of the Corner model potential is described in §6 where the results of Monte Carlo simulations are presented. The spherocylinder, with a length-to-breadth ratio of 3:1, is found to form isotropic, smectic A and possibly crystal B phases. The introduction of a central sphere into the molecule destroys the smectic A phase and replaces it with a nematic. This behaviour is consistent with the shape quadrupole of the spherocylindrical molecule with its embedded sphere. Where it is appropriate conclusions are drawn at the end of each section.

2. Liquid crystal mixtures (with J. W. Emsley and A. P. Singh)

Liquid crystal mixtures are widely used in most applications of liquid crystals especially in the area of displays where the composition of a multicomponent mixture is adjusted, usually empirically, to achieve a desired set of properties for a particular application. At

the same time investigations of liquid crystal mixtures, both experimentally and theoretically, are of fundamental interest especially for the insight they provide concerning the molecular interactions responsible for liquid crystal behaviour [1]. The simplest of such systems is a binary mixture composed of rod-like and spherical molecules which serve to dilute the anisotropic interactions between the molecular rods. Although the system is particularly simple the phase diagram is predicted to be rather intricate [2] as the example in figure 1 shows. Thus at low concentrations of the spherical component there is a nematic island surrounded by a biphasic region in which nematic and isotropic phases coexist. At higher concentrations the isotropic phase undergoes a transition to the biphasic system which then exists at all lower temperatures. The intriguing form of the phase diagram has been confirmed by computer simulation studies of model systems [3]. More recently a strikingly similar phase diagram has been reported for water droplets dispersed in the nematogen, 4-pentyl-4′-cyanobiphenyl (5CB) [4].

Since the high concentrations of the spherical component could not be readily achieved experimentally because the nematic phase was destroyed, attention was focused on the initial Henry's Law region of the phase diagram [5]. Here, the slope of the phase boundaries between the isotropic phase and biphasic region ($\beta_I = dT_I/dx$) and the biphasic region and nematic phase ($\beta_N = dT_N/dx$) were determined and compared with those predicted by theory. The experiments proved to be non-trivial because the quasi-spherical solutes, such as carbon tetrachloride, tended to have high vapour pressures and so tended to evaporate from the mixture. One solution to this problem was to employ solutes with higher molecular masses, for example, tetraethyltin [5]. However, the problem here is that

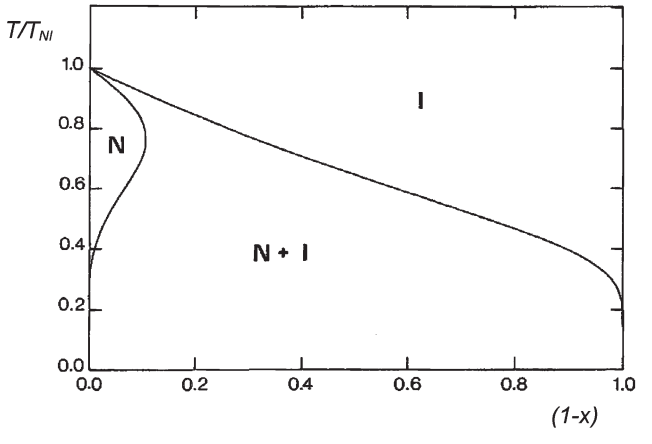

Figure 1. The phase diagram for a binary mixture of rod-like and spherical molecules predicted by molecular field theory.

the molecule is not even quasi-spherical in all of the conformations in which it can exist and so the anisotropic interactions will certainly influence the gradients β_I and β_N. Indeed the influence of the solute anisotropy proves to be rather large as the results of some novel experiments by Rosenblatt have shown [6]. In order to avoid the problems associated with the destruction of the nematic phase at moderately high solute concentrations, he determined the divergence temperature, T^*, by measuring the field-induced birefringence in the isotropic phase. This temperature is expected to be intermediate between T_N and T_I as well as to parallel both. In addition, theory [6, 7] shows that for a spherical solute, T^*_M for the mixture is proportional to that for the pure nematic T^*_A,

$$T^*_M = \phi_A \, T^*_A. \qquad (1)$$

Here, ϕ_A is the volume fraction of the nematic solvent in the mixture; this is used rather than the mole fraction to allow for any difference in the molar volume between solute and solvent. Two mixtures were investigated, both with 5CB as the nematic solvent; they differ, however, in that the solute for one mixture was carbon tetrachloride and for the other it was tetraethyltin. For the mixture with carbon tetrachloride T^*_M is linear with the volume fraction down to the relatively low value of 0.5 as predicted by equation (1). In contrast, the divergence temperature for the mixture with tetraethyltin exhibits a marked deviation from linearity in ϕ_A, with T^*_M being higher than that predicted by equation (1). It was suggested by Rosenblatt [6] that the flexible solute molecules might occupy channels parallel to the molecular long axes of the nematogenic solvent and so would disrupt the structure less than say the quasi-spherical molecules of carbon tetrachloride.

An alternative interpretation is that the solute, tetraethyltin, has a degree of anisotropy at least for some of its conformers, and that the anisotropic interactions between solute and solvent molecules will result in a smaller disruption to the nematic structure. To test this possibility we decided to investigate the orientational order of tetraethyltin in a nematic phase using deuterium NMR spectroscopy. To do this requires a deuteriated sample of tetraethyltin but this proved to be fairly easy to synthesize [8]. First, deuteriated ethyl bromide-d_5 was used to prepare the Grignard ethylmagnesium bromide-d_5. This was then reacted with tin tetrachloride to give the desired perdeuteriated tetraethyltin-d_{20}. We used Merck Phase V as the nematic solvent rather than the 5CB used in the pretransitional temperature measurements because it has a far larger nematic range; T_{CrN} is -5°C and T_{NI} is 75°C. The concentration of tetraethyltin-d_{20} in Phase V

was 2 wt % corresponding to the Henry's Law region of the phase diagram. The deuterium NMR spectrum was measured as a function of temperature using a Bruker CXP200 spectrometer at a frequency of 30.7 MHz with quadrature phase detection. A typical spectrum, taken deep in the nematic phase, is shown in figure 2; it consists of two quadrupolar doublets, and the lines of the inner doublet are further split by dipolar interactions between the deuterons. The observation of the quadrupolar splittings tells us immediately that the solute is orientationally ordered in the nematic solvent and so the solute cannot be behaving as a spherical solute. The dipolar couplings, taken together with the relative intensities of the inner and outer lines, show that the larger splitting is associated with the methylene deuterons and the smaller splitting with the methyl deuterons. The temperature dependence of the two quadrupolar splittings is shown in figure 3. They exhibit the expected decrease with increasing temperature, and at the nematic–isotropic phase transition the splittings, which are changing rapidly with temperature, then show a very weak dependence. This is associated with the onset of the biphasic region where the change of the orientational order with temperature is offset by that in the composition of the nematic phase [9].

The analysis of the two quadrupolar splittings and their variation with temperature is a difficult task. This difficulty results from the rotation of the methyl groups about the carbon–tin bonds which means that the molecule adopts a range of conformations that will be orientationally ordered to different extents in the nematic phase. The conformers generated by torsional rotations of the methyl groups can be visualized, within the rotational isomeric state model, in the following way. The tin atom and the four carbon atoms bonded to

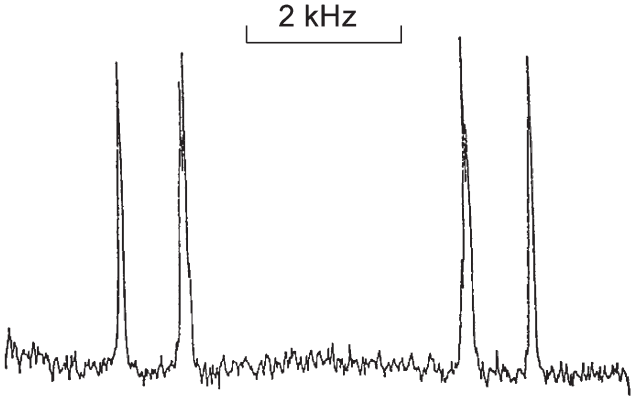

Figure 2. The deuterium NMR spectrum of tetraethyltin-d_{20} dissolved in nematic Phase V at a shifted temperature, $T_{NI}-T$, of 42.4°C.

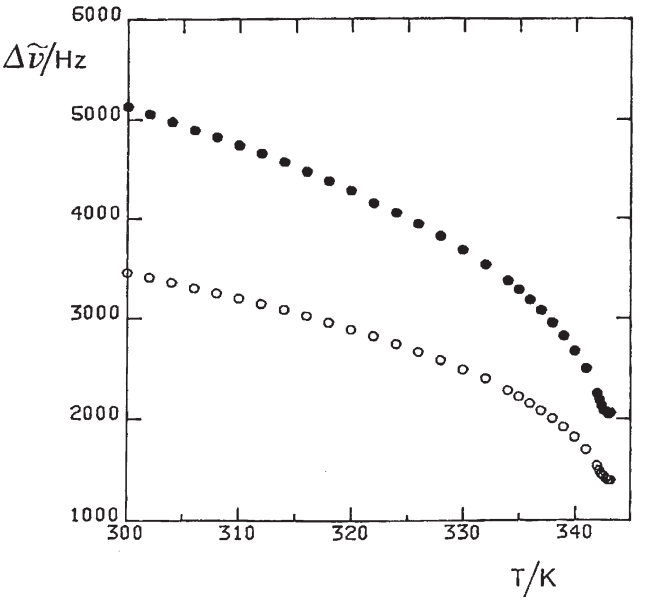

Figure 3. The temperature dependence of the quadrupolar splittings for the methyl (○) and methylene (●) deuterons in tetraethyltin-d_{20} dissolved in nematic Phase V.

it constitute a rigid tetrahedral core. It is the four methyl groups attached to these carbon atoms that rotate, together with the methylene deuterons, about the C–Sn bonds. The conformational energy will be a minimum at the three positions of the methyl group midway between two carbon–tin bonds. These conformations can be thought of as *trans*, *gauche*(+) and *gauche*(−) with respect to one of the pentane-like fragments and will differ in energy. The shapes of the conformations will also be different and the nematic environment will stabilize these to different degrees, depending on the anisotropy of the conformer (see § 3). The most anisotropic conformer is shown in figure 4, it has S_4 symmetry and can be viewed as being formed by linking together two pentane-like chains, each in an all-*trans* conformation, orthogonal to each other and at the central atom which would be tin. The anisotropy of this conformer can be calculated from the additive potential model [10] where the anisotropic interaction tensor is assumed to be the tensorial sum of those for certain segments constituting the molecule [see equation (17)]. If these segments are taken to be the C–Sn and C–C bonds and if the $C\hat{C}C$ and $C\hat{C}Sn$ bond angles are tetrahedral, then the anisotropy in the interaction tensor for the S_4 conformer vanishes [11]. This result is clearly in conflict with the anisotropic shape of the conformer. One solution to this paradox is to include the so-called chord segments suggested by Marcelja [12] for membranes and then used by Photinos *et al.* [13] for

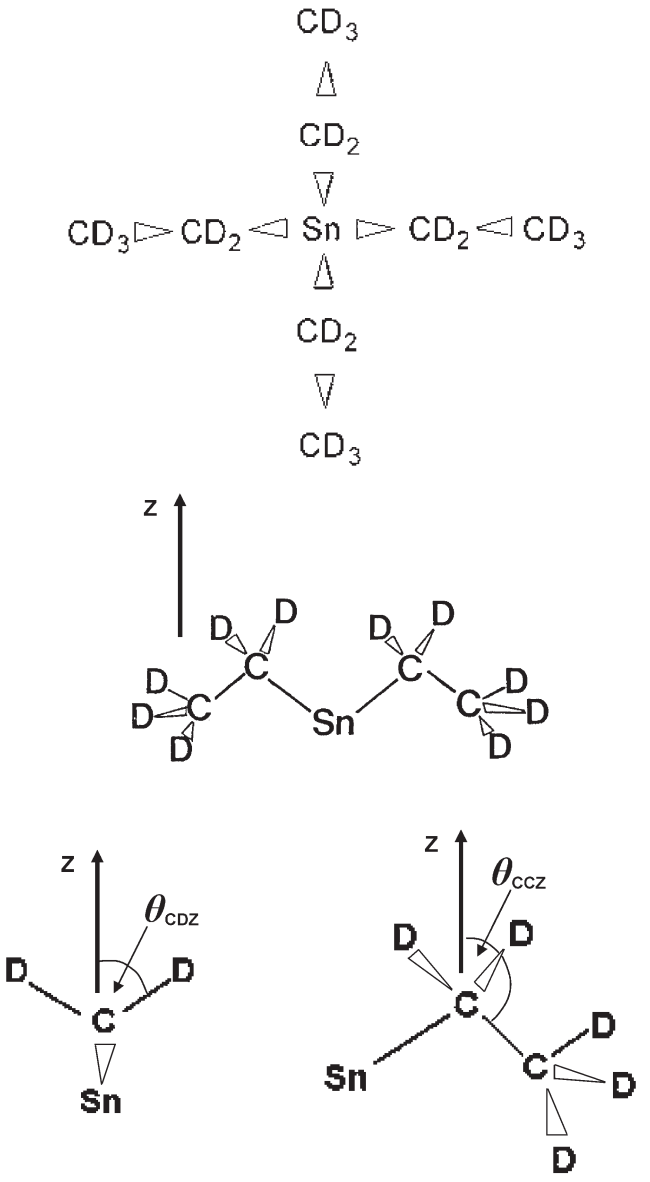

Figure 4. The geometrical and conformational structure of tetraethyltin.

nematics, where a chord links the mid points of neighbouring bonds. In the case of the S_4 conformer this results in an anisotropic tensor with cylindrical symmetry about the symmetry axis of the conformer, as expected.

The S_4 conformation has a unique axis, z, and so at the second rank level its orientational order is characterized solely by S_{zz}. The quadrupolar splittings are proportional to this order parameter together with certain geometrical factors; the angles defining these are shown in figure 4. The splittings are given by [14]

$$\Delta\tilde{\nu}_{CD_3} = (3/4)q_{CD}S_{zz}\left(3\cos^2\theta_{CDz} - 1\right) \qquad (2)$$

and

$$\Delta\tilde{\nu}_{CD_3} = (3/8)q_{CD}S_{zz}\left(3\cos^2\theta_{CCz} - 1\right)\left(3\cos^2\alpha - 1\right), \qquad (3)$$

where q_{CD} is the quadrupolar coupling for an aliphatic deuteron, normally taken to be 168 kHz. The dependence of the two quadrupolar splittings on the angles θ_{CDz} and θ_{CCz} leads to another problem in the limit that the $C\hat{C}C$ and $C\hat{C}Sn$ bond angles are tetrahedral, for then θ_{CDz} and θ_{CCz} are equal to 54.74° and 180°–54.74° which are the magic angle and its supplement. Since $P_2(\cos\beta)$ is zero for the magic angle, the quadrupolar splittings would vanish identically. The fact that they do not would be consistent with deviations of the bond angles from the tetrahedral value. This is known to be the case for alkane fragments in mesogenic molecules such as 4-alkyl-4′-cyanobiphenyl [15] and has also been observed for alkyl-substituted tin compounds [16]. If we assume that the angles θ_{CDz} and θ_{CCz} do deviate from the magic angle and its supplement then we can proceed with our analysis.

The S_4 symmetry of the conformer means that the ratio of the two quadrupolar splittings is determined solely by the geometry of the conformer and so should be independent of temperature. This proves to be the case over a nematic range of almost 41°C, for $\Delta\tilde{\nu}_{CD_2}/\Delta\tilde{\nu}_{CD_3}$ is 1.47 ± 0.01, which provides some support for our assumption of a dominant conformer with S_4 symmetry. To go further with the analysis is a problem because there are just two pieces of information, $\Delta\tilde{\nu}_{CD_2}$ and $\Delta\tilde{\nu}_{CD_3}$, but four unknowns in the model; that is, the order parameter and the three angles. The splittings in the limit of perfect orientational order ($S_{zz} = -½$) can be estimated by extrapolating to absolute zero by using the Haller plot [17]. In this limit the only unknowns determining the two quadrupolar splittings are the three angles, α, θ_{CDz} and θ_{CCz}. It is reasonable to assume that α has the tetrahedral value of 109.47° and this then leads to $\theta_{CDz} = 57.2°$ and $\theta_{CCz} = 120.1°$, provided the quadrupolar splittings are opposite in sign; θ_{CDz} is close to half of the tetrahedral value as might be expected and θ_{CCz} is in accord with the value of $C\hat{C}Sn$ found from X-ray studies. Armed with this geometric information the temperature dependence of the order parameter S_{zz} can be determined and this is shown in figure 5. First, we note that the order parameter is negative; this follows from the disc-like shape of the S_4 conformation which will tend to align with the S_4 axis orthogonal to the director. Secondly, at the nematic–isotropic transition S_{zz} is about −0.13 and then decreases to −0.33. These are significantly large values which demonstrate the relatively high orientational order of tetraethyltin in the nematic host. It is clear now that the behaviour found for the concentra-

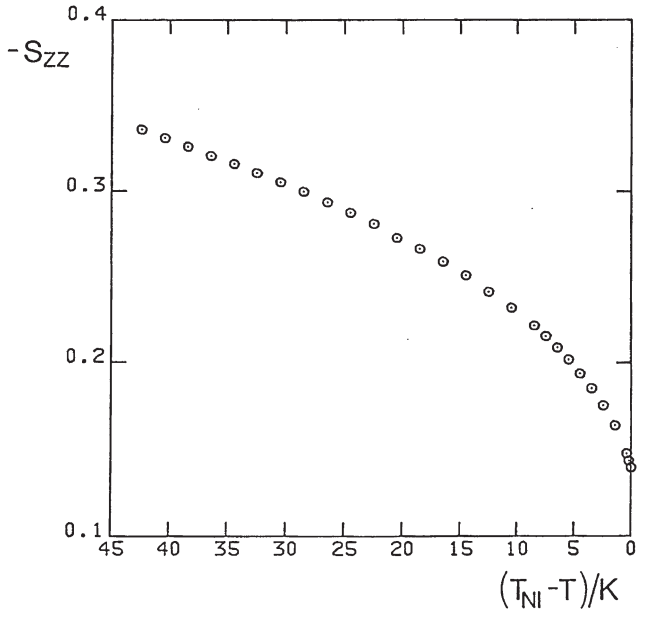

Figure 5. The dependence of the order parameter, S_{zz}, for tetraethyltin-d_{20} dissolved in nematic Phase V on the shifted temperature, $T_{NI}-T$, determined assuming a dominant S_4 conformation.

tion dependence of the divergence temperature results from the anisotropic nature of the solute molecule. According to theory the divergence temperature for the mixture is given by [7]

$$T^*_M = \phi_A\ T^*_A + (1-\phi_A)T^*_B, \qquad (4)$$

where T^*_B is the divergence temperature for the disc-like component. The data for tetraethyltin in 5CB is in good agreement with this theoretical prediction and so provides further evidence for the anisotropic nature of the guest molecule. By fitting the expression in equation (4) to the experimental data we find a value for the divergence temperature of tetraethyltin of -136°C, which seems reasonable and proves to be consistent with the orientational order parameter determined for tetraethyltin in Phase V. Finally we note that, although this quantitative conclusion is satisfactory, there is an alternative analysis of the data; this is based on the additive potential model and includes other conformations in which the pentane-like fragments adopt *gauche* as well as *trans* conformations [11].

3. Multipodes—a molecular field theory (with J. W. Essex and T. H. Payne)

The growth in the complexity of mesogenic molecules has been one of the exciting developments in the area of thermotropic liquid crystals [18]. One group of such novel compounds is formed by dendritic liquid crystals in which a highly branched and flexible dendritic structure is decorated with mesogenic groups, normally attached to the perimeter of the dendrimer [19]. The simplest member of this class of compound is the zeroth generation dendrimer or multipode in which mesogenic groups are linked through flexible spacers to a central atom or relatively rigid molecular group [20]. Possibly the first tetrapodes were described by Eidenschink *et al.* [21] in which mesogenic groups are joined to a central carbon atom through relatively short chains containing an ester linkage. The compound with three-ring mesogenic groups forms both smectic A and smectic B phases. In later studies, compounds with a central silicon atom linked to four mesogenic groups with flexible spacers containing siloxane units and methylene groups were also found to form liquid crystals [20]. When the mesogenic groups are linked terminally to the chains there is a tendency to form smectic A phases [22]. In contrast, multipodes with laterally linked mesogenic groups tend to exhibit nematic phases [23]. Of particular interest is the claim that certain tetrapodes form the elusive biaxial nematic phase [24]. It is clearly of considerable importance to explore the relationship between the nematic behaviour and the molecular structure. We have, therefore, attempted to investigate this relationship theoretically using a molecular field approach and a model tetrapode in which the mesogenic groups are linked, both terminally and laterally, by alkyl chains to a central carbon atom.

The theory must account for two essential features of a multipode, one is the flexibility of the branched core and the other is the anisotropic interactions of the mesogenic groups. As a result of both features the overall molecular anisotropy changes significantly with the conformational state. This behaviour is analogous to that for liquid crystal dimers where, as the conformation of the chain linking the two mesogenic groups changes, so too does their relative orientation and the anisotropy of the dimer. Molecular field theories of such effects have been developed and these tend to rely on the rotational isomeric state model [25] to describe the conformation of the spacer [10, 12, 13, 26]. In this the chain segments are taken to exist in discrete conformations, *trans*, *gauche*(+) and *gauche*(−). Although this simplifies the calculations it is unrealistic since conformational fluctuations in the minima of the torsional potentials do influence the relative orientations of the mesogenic groups, especially for long spacers. To allow for this effect in the theory is relatively straightforward. However, the calculations become considerably more involved and it is no

longer possible to include all conformational states which, as we shall see, must be sampled using a biased Monte Carlo algorithm [27]. The methodology developed for dimers should certainly be applicable to multipodes and, in principle, to higher generation dendrimers. Here we sketch the basic theory and then use it to predict certain transitional behaviour of the tetrapodes.

The starting point for the molecular field theory is the energy of a molecule in a particular conformation and orientation. Here the conformation is defined in terms of the torsional angles, ϕ, along the chains and these are denoted collectively by $\{\phi\}$. The molecular orientation is given by the spherical polar angles, β and α, defining the orientation of the director in a frame fixed in a rigid part of the molecule; these are denoted by ω. The energy is written as the sum of two parts

$$U_{\rm tot}(\{\phi\}\omega) = U_{\rm int}(\{\phi\}) + U_{\rm ext}(\{\phi\}\omega), \qquad (5)$$

where the first part depends only on the molecular conformation and the second on both the orientation as well as the conformation [28]. Formally, such a separation of the total single molecule energy is always possible, and so what is important is the physical significance of the two terms. The energy, $U_{\rm int}(\{\phi\})$, is taken to be the conformational energy that would obtain in the isotropic phase. The other contribution, $U_{\rm ext}(\{\phi\}\omega)$, is the anisotropic potential responsible for the alignment of the molecule with respect to the director; it necessarily vanishes in the isotropic phase. The torsional potential for each chain segment is taken to have the Ryckaert–Bellemans form

$$\begin{aligned} U(\phi) = {} & V_0 + (V_1/2)[1+\cos(\phi+f_1)] \\ & + (V_2/2)[1-\cos(2\phi+f_2)] \\ & + (V_3/2)[1+\cos(3\phi+f_3)], \end{aligned} \qquad (6)$$

where the f_i are phase shifts [29]. The anisotropic potential is taken from the molecular field theory for rigid molecules in a uniaxial phase [30] and is given by

$$U_{\rm ext}(\{\phi\}\omega) = -\sum (-)^m X_{2m}(\{\phi\}) C_{2-m}(\omega), \qquad (7)$$

where $C_{2-m}(\omega)$ is a modified spherical harmonic and determines how the energy changes as the molecule rotates in a fixed conformation. The strength of the molecular field is contained in the tensor X_{2m}; it depends on the anisotropy of the molecule and so on the conformation $\{\phi\}$. It is also determined by the orientational order of the nematic phase and we shall return to this dependence later.

The energy is then used to evaluate a number of average quantities but rather than deal with each of these explicitly we give the result for a general property $B(\{\phi\}\omega)$ which is a function of both the conformation and the orientation of the molecule. The average, $\langle B\rangle$, of this property is given by

$$\langle B\rangle = \int\int B(\{\phi\}\omega) P(\{\phi\}\omega) {\rm d}\{\phi\}{\rm d}\omega \qquad (8)$$

where $P(\{\phi\}\omega)$ is the singlet conformational and orientational distribution function. This distribution is related to the total energy by the usual Boltzmann factor, that is

$$P(\{\phi\}\omega) = \exp(-U_{\rm tot}(\{\phi\}\omega)/k_{\rm B}T)/Q_{\rm tot} \qquad (9)$$

where the conformational–orientational partition function is given by

$$Q_{\rm tot} = \int\int \exp(-U_{\rm tot}(\{\phi\}\omega)/k_{\rm B}T){\rm d}\{\phi\}{\rm d}\omega. \qquad (10)$$

It is of interest to obtain the conformational distribution from this result irrespective of the molecular orientation. This is obtained from equation (9) by integrating over the angles ω which gives

$$P(\{\phi\}) = Q_{\rm ext}(\{\phi\})\exp(-U_{\rm int}(\{\phi\})/k_{\rm B}T)/Q_{\rm tot}. \qquad (11)$$

Here $Q_{\rm ext}(\{\phi\})$ is the orientational partition function for the conformer $\{\phi\}$. $Q_{\rm tot}$ can be written in a similar form, namely,

$$Q_{\rm tot} = \int Q_{\rm ext}(\{\phi\})\exp(-U_{\rm int}(\{\phi\})/k_{\rm B}T){\rm d}\{\phi\}. \qquad (12)$$

This shows that in the liquid crystal phase the probability of a given conformer is changed by the orientational partition function for that conformer. This means that the anisotropic conformers will be favoured in the liquid crystal phase, as expected, but in a way that can be quantified.

The average, $\langle B\rangle$, can be written in a similar form by performing the integration over ω; this gives

$$\langle B\rangle = \frac{\int \langle B(\{\phi\})\rangle_\omega Q_{\rm ext}(\{\phi\})\exp(-U_{\rm int}(\{\phi\})/k_{\rm B}T){\rm d}\{\phi\}}{\int Q_{\rm ext}(\{\phi\})\exp(-U_{\rm int}(\{\phi\})/k_{\rm B}T){\rm d}\{\phi\}}, \qquad (13)$$

where $\langle B(\{\phi\})\rangle_\omega$ is the orientational average of $B(\{\phi\}\omega)$ for a given conformation $\{\phi\}$. This orientational average is given by

$$\langle B(\{\phi\})\rangle_\omega = \int B(\{\phi\}\omega)\exp(-U_{\rm ext}(\{\phi\}\omega)/k_{\rm B}T){\rm d}\omega/Q_{\rm ext}(\{\phi\}). \qquad (14)$$

The average $\langle B\rangle$ given in equation (13) can be viewed as the conformational average of the property $\langle B(\{\phi\})\rangle_\omega$ for each conformer. The challenge now is to evaluate the integrals in equation (13), but this cannot be achieved analytically and the continuous nature of the torsional variables $\{\phi\}$ means that not all conformations can be included in the average. This

requires the conformational variables to be sampled randomly, and this is best done with an inbuilt bias to give a conformational distribution appropriate for the isotropic phase [27]. The average in the isotropic phase would then be given by

$$\langle B\rangle = \lim_{N\to\infty} \sum_{i}^{N} \langle B(\{\phi_i\})\rangle_\omega / N \qquad (15)$$

where $\{\phi_i\}$ denotes a particular conformation for an accepted Monte Carlo move. As we have seen, the conformational distribution in the nematic phase differs from that in the isotropic phase, see equation (11), and to compensate for this difference equation (15) must be modified [27]. The corrected form is

$$\langle B\rangle = \lim_{N\to\infty} \left[\frac{\sum_{i}^{N} \langle B(\{\phi_i\})\rangle_\omega Q_{\text{ext}}(\{\phi_i\})}{\sum_{i}^{N} Q_{\text{ext}}(\{\phi_i\})} \right] \qquad (16)$$

which is analogous to that encountered in umbrella sampling [31]; it will be effective provided the distributions in the two phases do not differ significantly.

An essential part of the model is the explicit relationship between the strength tensor, $X_{2m}(\{\phi\})$, and the molecular conformation, $\{\phi\}$. There is a variety of ways in which these can be related [10, 12, 13, 26] and many rely on a segmental approximation; that is, the tensor $X_{2m}(\{\phi\})$ is assumed to be a tensorial sum of certain contributions from segments within the molecule,

$$X_{2m}(\{\phi\}) = \sum_j X^j_{2m}(\{\phi\}). \qquad (17)$$

Here the segmental contributions, $X^j_{2m}(\{\phi\})$, are expressed in a common molecular frame where they still depend on the molecular conformation. This dependence is made explicit simply by transforming from the segmental frame, where the interaction tensor is a constant, to the common molecular frame via

$$X^j_{2m}(\{\phi\}) = \sum_n X^j_{2n} D^2_{nm}\big(\Omega_j(\{\phi\})\big). \qquad (18)$$

Here, $D^2_{nm}\big(\Omega_j(\{\phi\})\big)$ is a Wigner rotation matrix, where $\Omega_j(\{\phi\})$ denotes the Euler angles relating the segmental and molecular frames, these angles depend on the molecular conformation. For calculations on the tetrapodes the segments associated with the linking chains are ignored and only contributions from the highly anisotropic mesogenic groups are included. In addition, it is assumed that the mesogenic groups are cylindrically symmetric about the group long axis. This enables equation (17) to be written as

$$X_{2m}(\{\phi\}) = \sum_j X^j_{20} C_{2m}\big(\omega_j(\{\phi\})\big), \qquad (19)$$

where ω_j denotes the spherical polar angles of the symmetry axis for group j in the molecular frame.

Our numerical implementation of the molecular field theory relies heavily on the use of the code BOSS (Biological and Organic Simulation System) [32]. This generates the conformations from a given molecular structure, calculates the conformational energies and samples the conformational states using a Monte Carlo technique appropriate for the isotropic phase. These accepted conformations are then used to determine a range of average properties via equation (16); of special interest here is the order parameter, $<P_2>$, of the mesogenic group together with those quantities required to determine the Helmholtz free energy difference

$$A_{\text{N}} - A_{\text{I}} = -\langle U_{\text{ext}} Q_{\text{ext}}\rangle/2\langle Q_{\text{ext}}\rangle - k_{\text{B}}T \ln(\langle Q_{\text{ext}}\rangle/4\pi). \qquad (20)$$

The nematic–isotropic transition is located by determining when this difference vanishes. The temperature enters the simulations via the scaled variable $X^*(\equiv X_{20}/k_{\text{B}}T)$ and it is the value of this variable that is determined at the transition. However, as we have seen, the strength tensor, X_{2m}, also depends on the orientational order of the phase. In consequence X^*_{NI} will not depend on temperature alone but will also vary with the order parameter for the mesogenic groups, $<P_2>_{\text{NI}}$, at the transition. This relationship is provided by molecular field theory as

$$X^*_{\text{NI}} = (\varepsilon/k_{\text{B}}T_{\text{NI}})\langle P_2\rangle_{\text{NI}}. \qquad (21)$$

Although the proportionality constant, ε, is not known, it is determined, in principle, by the anisotropy of a mesogenic group.

The simulations were performed for the tetrapodes shown in figure 6, with the mesogenic groups attached both terminally and laterally to the flexible alkyl chains through ether linkages. One of our prime interests is in the variation of the nematic–isotropic transition temperature with the number of groups, n, in the chain linking a mesogenic group to the central carbon atom and the nature of the attachment. This dependence of the scaled transition temperature, $T^*_{\text{NI}}(\equiv k_{\text{B}}T_{\text{NI}}/\varepsilon)$, is shown in figure 7 for both groups of tetrapodes; that is, with terminal and lateral modes of attachment. One striking feature of the results is that the tetrapodes with laterally attached mesogenic groups have a higher nematic–isotropic transition than those with terminal attachments. This difference is especially large for short chains (n=4) and then decreases with the length of the alkyl chain until it vanishes when n is 12. Individually,

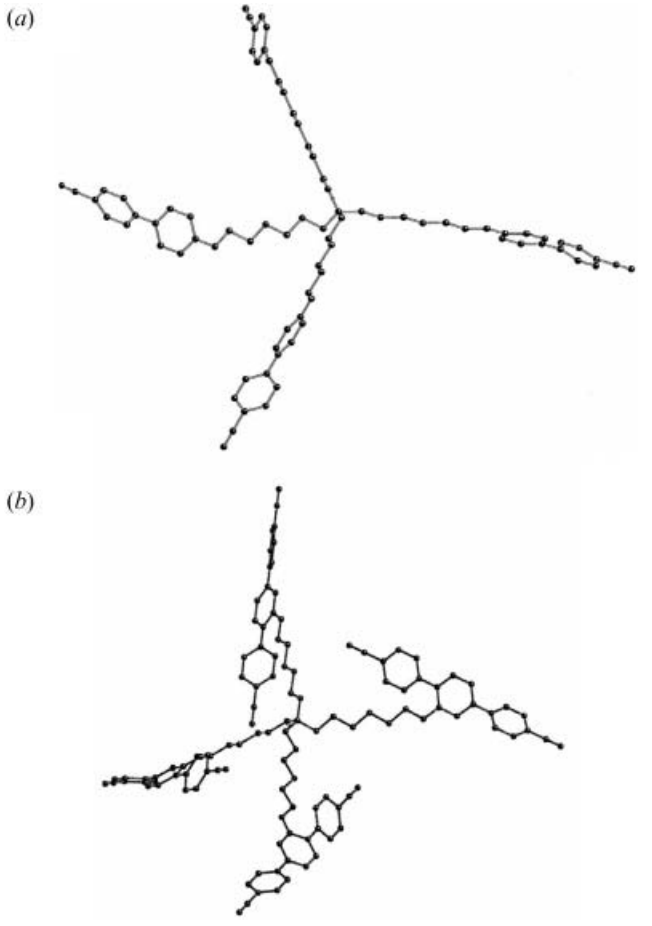

Figure 6. The molecular structures of the two classes of tetrapodes studied in the molecular field calculations: (*a*) with cyanobiphenyl groups attached terminally and (*b*) with dicyanoterphenyl groups attached laterally.

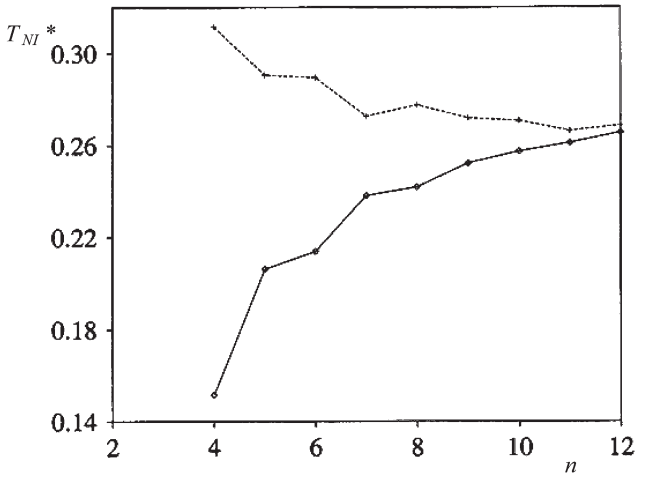

Figure 7. The variation with spacer length, n, of the scaled nematic–isotropic transition temperature, $T^*_{NI}(\equiv k_B T_{NI}/\varepsilon)$, for tetrapodes having terminally ($\diamond$) and laterally (+) attached mesogenic groups.

T^*_{NI} for the lateral tetrapodes decreases with chain length while that for the terminal tetrapodes increases.

These results can be understood in a relatively simplistic manner in terms of the behaviour of certain limiting structures. Thus when the flexible core of the tetrapode places no constraints on the relative orientations of the mesogenic groups the system will behave as four independent mesogenic groups. In this limit the nematic–isotropic transition will be that predicted by the Maier–Saupe theory for which T^*_{NI} is 0.2203 [33]. This value is very close to that found for both classes of tetrapodes when the chain length $n=12$. At the other extreme it might be envisaged that the core is rigid and that the mesogenic groups have fixed relative orientations. If, for example, the four groups had a tetrahedral arrangement then at second rank level the anisotropy has vanished and so T^*_{NI} would also vanish. This suggests that to some extent the terminal tetrapodes with short alkyl chains tend to adopt conformations for which the anisotropies of the mesogenic groups tend to cancel. This would be consistent with the ground-state conformation of the flexible core. Conversely, if the rigid conformation allows the four mesogenic groups to be aligned parallel to each other then the molecular anisotropy will be four times that for a single mesogenic group. The nematic–isotropic transition temperature is then predicted by molecular field theory to be four times that for a single mesogen [34]. This would then suggest that in the lateral tetrapodes with short chains the mesogenic groups tend to be arranged parallel to each other.

The predicted values of T^*_{NI} for the two classes of tetrapodes do exhibit a subtle odd–even behaviour, with odd members of the homologous series falling on one smooth curve and even members on another. This effect is well-known for liquid crystal dimers where the even members of a series tend to have higher transition temperatures than neighbouring odd members, as we shall see in § 4. The lateral multipodes exhibit the same behaviour although the difference is less pronounced than for the dimers. In contrast, the terminal tetrapodes exhibit the reverse behaviour, with the even members having smaller nematic–isotropic transition temperatures than their odd neighbours. Since the factors controlling T^*_{NI} for flexible molecules are complicated, and because the odd–even behaviour predicted for the tetrapodes is subtle, we shall not attempt to provide an intuitive explanation here.

The other quantity of interest is the magnitude of the orientational order of the nematic phase formed by the tetrapodes. A measure of this is provided by the value of the second rank order parameter of a mesogenic group, $<P_2>_{NI}$, at the transition. The dependence of this order

parameter on the alkyl chain length for the terminal and lateral tetrapodes is shown in figure 8. It is immediately apparent that the results for the terminal tetrapodes show initially a strong odd–even effect with the values for the even chains being higher than for the odd. However, this alternation is rapidly attenuated and has virtually vanished when n is greater than 9. In contrast the order parameters for the lateral tetrapodes do not exhibit an odd–even effect although $<P_2>_{NI}$ does decrease with increasing chain length and tends to the same limiting value as the terminal tetrapodes of approximately 0.44. This value is essentially the same as that predicted by the Maier–Saupe theory for rigid, cylindrically symmetric molecules which gives $<P_2>_{NI}$ as 0.429 [33]. This essential equality of the order parameters is to be expected because for long alkyl chains the mesogenic groups of the tetrapodes are not directly correlated and so behave like a collection of monomers. The observation for the tetrapodes with short chains that the order parameter is higher than that predicted for single mesogens is of considerable interest. Similar behaviour is found for liquid crystal dimers with even spacers [35] and has been attributed to increases in the probabilities of anisotropic conformers on passing from the isotropic to the nematic phase. It is possible that the same mechanism applies for the tetrapodes; the simulations suggest that for lateral attachment the conformational change would need to be monotonic in the spacer length, whereas for terminal attachment the change would be greater for even than for odd chains.

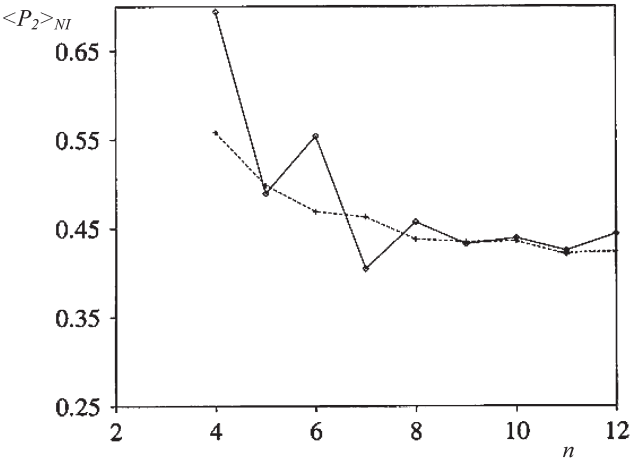

Figure 8. The dependence of the orientational order parameter for a mesogenic group, $<P_2>_{NI}$, at the transition on the chain length for the terminal (◇) and lateral (+) tetrapodes.

4. Liquid crystal dimers with long spacers (with F. J. Farrand)

Liquid crystal dimers, in which two mesogenic groups are linked by a flexible spacer, constitute a novel class of materials. They were discovered by Vorländer [37] who found that the transitional properties depended, in a major way, on both the length of the spacer and the parity of the number of atoms in it. Despite the novelty of this behaviour the discovery appears to have been forgotten, and it was not until many years later that the intriguing transitional properties were rediscovered [38]. Now, the interest in liquid crystal dimers was not lost and there has been considerable activity, both in the phases that they form and how these depend on the nature of the mesogenic groups as well as the spacer. One of the longest series of homologues, made at the start of such investigations, was the α,ω-bis(4-cyanobiphenyl-4′-yloxy)alkanes [39]. They were found to form only nematic phases, at least for the early members of the series up to the dodecane spacer. The variation of the nematic–isotropic transition temperature and the transitional entropy, $\Delta S/R$, with the number of atoms, n, in the spacer is shown in figure 9. Here n is two more than the number of carbon atoms because of the two oxygen atoms constituting the ether links. The transition temperatures clearly exhibit a strong alternation, with the even homologues having a higher value than their odd neighbours, see figure 9 (*a*). The alternation is particularly dramatic at the start of the series where T_{NI} for the dimer with the $n=4$ spacer is over 140°C higher than that for $n=3$. This major alternation is, however, rapidly attenuated as the chain length increases, although the T_{NI} values still differ by about 10°C for the homologues with $n=13$ and 14. The transitional entropy, $\Delta S/R$, shown in figure 9 (*b*) also exhibits a strong alternation but, unlike the transition temperature, this does not appear to be attenuated as the spacer length increases. The transitional entropy for dimers with odd spacers is comparable with that for monomers, while $\Delta S/R$ for dimers with even spacers is about three times larger. This considerable difference in the transitional entropy suggests that the orientational order for even dimers is significantly greater than that for odd dimers and NMR studies have shown this to be the case [35].

It is tempting to suppose that this difference in behaviour for even and odd liquid crystal dimers originates from their difference in shape. Thus for the spacer in its all-*trans* conformation the even dimers have a zig-zag shape in which the mesogenic groups are parallel. In contrast the odd dimers have a bent or banana shape in which the mesogenic groups are inclined to each other. However, this cannot be the entire explanation for it suggests that the even dimers

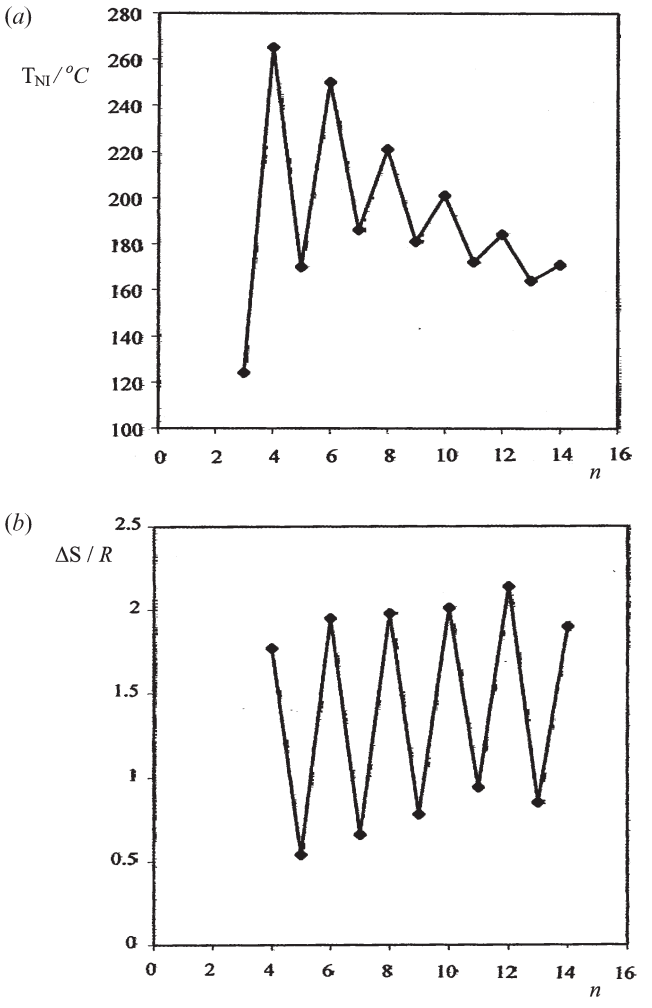

Figure 9. The variation of (*a*) the nematic–isotropic transition temperature, T_{NI}, and (*b*) the transitional entropy, $\Delta S/R$, with the number of atoms, *n*, in the spacer for the early members of the α,ω-bis(4-cyanobiphenyl-4′-yloxy)alkanes (CBO(*n*-2)OCB).

with their parallel mesogenic groups should behave like monomers whereas the odd dimers with their bent structures should be more weakly ordered. In fact as far as the transitional entropy is concerned the odd dimers behave like the monomers and the even dimers have a considerably higher transitional entropy. What we have ignored so far is the flexibility of the spacer linking the mesogenic groups which allows the molecules to exist in many conformational states with differing anisotropies. In addition, the conformational distribution will change when the phase undergoes a transition from isotropic to nematic with the more anisotropic conformers being favoured in the nematic phase, see equation (11). The ability of the change of phase to modify the conformational distribution will, of course, depend on the conformational energy of the anisotropic conformers. This proves to be higher for odd dimers than for even, so that the conformational changes will be larger for the even than the odd dimers. As a consequence the increase in the fraction of the more anisotropic conformers will enhance the order of the nematic phase to a greater extent for the even dimers in comparison with the odd.

Theories for flexible mesogenic molecules based on the molecular field approximation have been developed, and the essential features of these are described in § 3. A key aspect of such theories is the approach used to describe the conformational state of the spacer. In that used for the tetrapodes the conformation is defined in terms of the torsional angles, ϕ, along the spacers, which constitute a set of continuous variables; the conformational energy is then calculated from the Ryckaert–Bellemans potential, see equation (6). At the other extreme, in the rotational isomeric state model, the torsional angles are only allowed to take three discrete values, corresponding to the *trans*, *gauche*(+) and *gauche*(−) conformations of a link in the chain. In its simplest form the conformational energy is given by

$$U_{\text{int}}(\{\phi\}) = n_g E_{tg}, \tag{22}$$

where n_g is the number of *gauche* links in the spacer and E_{tg} is the energy difference between a *trans* and a *gauche* link [25]. The transitional properties for liquid crystal dimers using both discrete and continuous models for the conformational states have been calculated as a function of the spacer length [27]. The results for the scaled nematic–isotropic transition temperature, $T_{NI}/T_{NI}^{(6)}$, and the transitional entropy, $\Delta S/R$, are shown in figures 10 (*a*) and 10 (*b*), respectively. The striking feature of the two plots is that the discrete model predicts a far greater alternation in both $T_{NI}/T_{NI}^{(6)}$ and $\Delta S/R$ than the continuous model. Indeed the alternation in $\Delta S/R$ is predicted to increase with the spacer length by the discrete model, whereas the continuous model predicts that the odd–even effect in the transitional entropy is attenuated; this difference in behaviour is most pronounced when the spacer is long. The alternation in the transition temperature is predicted to be rapidly attenuated by the continuous model and to decrease slightly with increasing spacer length. In contrast the discrete model predicts a strong alternation in T_{NI} even for the longest spacer. This difference in behaviour predicted by the two conformational models results from the maintenance of the orientational correlations between the mesogenic groups in the discrete model, whereas for the continuous model the torsional fluctuations about the energy minima result in a more effective loss of orientational correlations. In order to test the differing predictions of

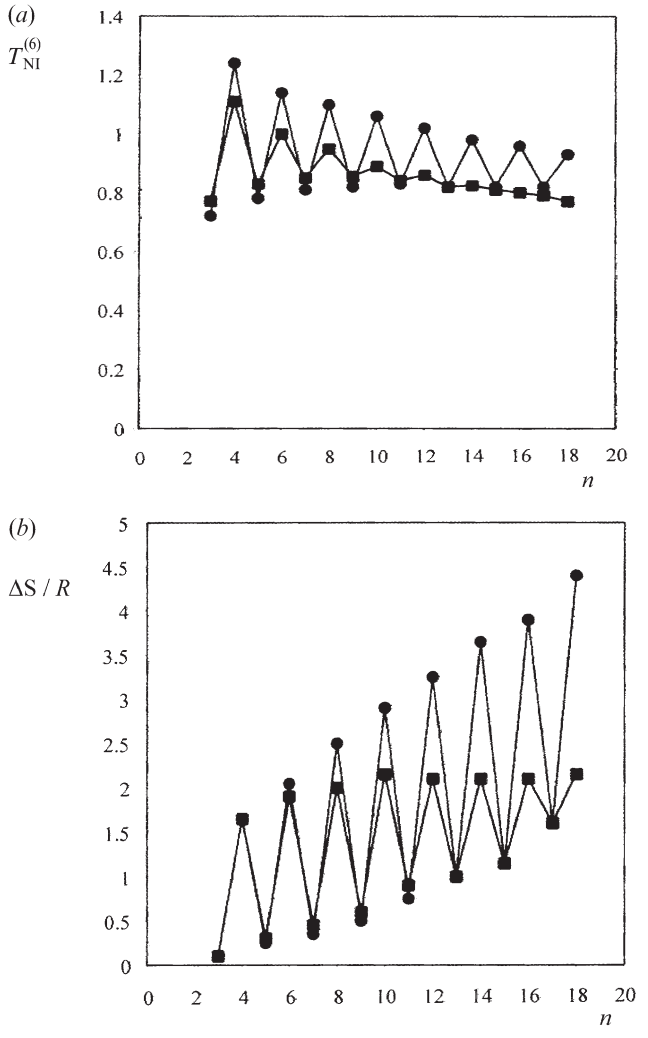

Figure 10. The predicted dependence of (*a*) the scaled nematic–isotropic transition temperature, $T_{NI}/T_{NI}^{(6)}$, where the superscript (6) denotes the value for the six spacer dimer, and (*b*) the transitional entropy, $\Delta S/R$, on the spacer length, *n*. The results obtained using the rotational isomeric state model are denoted by –●– and those for the continuous model are shown as –■–.

the two models, and to see which provides the most realistic description of the chain conformations, we have synthesized liquid crystal dimers with longer spacers.

The homologues of the α,ω-bis(4-cyanobiphenyl-4′-yloxy)alkanes that have been reported were prepared from 4-hydroxy-4′-cyanobiphenyl and the α,ω-dibromoalkane via a Williamson synthesis [39]. The α,ω-dibromoalkanes are commercially available for chain lengths of up to 12 carbon atoms. The dibromides are conveniently prepared from the corresponding alkane diols and although these were not commercially available two diacids from which they could be synthesized were. These diacids were brassylic acid and tetradecanedioic acid which, on reduction, gave 1,13-tridecanediol and 1,14-tetradecanediol, respectively. To proceed to longer spacers it was necessary to synthesize either the α,ω-diols directly or the α,ω-diacids; this proved to be a non-trivial task and a range of strategies had to be employed in order to extend the series to give spacers containing from 14 to 24 atoms. The routes to the α,ω-diacids and the α,ω-diols involved the symmetric addition of groups to a difunctional alkene or alkane. We found that no one route would produce all of the chain lengths that were required and eventually three distinct synthetic routes had to be employed [40–42].

The first of these is shown in figure 11. It involves the nucleophilic substitution of 1,4-dibromobut-2-ene by 1,3-cyclohexanedione to form 1,4-bis(1,3-cyclohexanedione)but-2-ene. Then, under Wolff–Kishner reaction conditions, one of the carbonyls on each ring is reduced and the other is hydrolysed to the acid. This gives the α,ω-diacid and the double bond at the centre of the molecule is reduced by hydrogenation. Unfortunately this route could only be used for 1,16-hexadecanedioic acid because the 1,4-dibromobut-2-ene is necessary to create the stabilizing allylic group.

The second route was more effective and allowed us to synthesize three diacids, namely those with 19, 20 and 21 carbon atoms in the chain. The synthetic route is shown for 1,21-heneicosanedioic acid in figure 12 and is based on 1-morpholino-1-cyclohexene. This is reacted with azelaoyl chloride and leads to a cyclic ketone which is then saponified to give the sodium salt of the diacid. The two carbonyl groups remaining in the chain must then be reduced, again using Wolff–Kishner conditions, to give the desired α,ω-diacid. To obtain the other chain lengths the reaction was performed with 1-morpholino-1-cyclopentene which gave 1,19-nonadecanedioic acid. The other member of the series, 1,20-eicosanedioic acid, was prepared using 1-morpholino-1-cyclopentene and sebacoyl chloride. In practice this route proved to be problematic partly because during the saponification of the cyclic ketone the chain was also cleaved at the carbonyl group, at least for certain chain lengths.

The final route [42] that we have employed to synthesize the α,ω-diols is shown in figure 13; it does not involve the reduction of an α,ω-diacid but proceeds directly to the α,ω-diol via the hydrolysis of the α,ω-diacetate. This diester is prepared by first making the acetate of 1-chloro-4-butyl alcohol. In the next step the chlorine is replaced by iodine and the resulting iodo-ester is reacted with a di-Grignard reagent made from 1,7-dibromoheptane. This gives the 1,15-pentadecanyl-diacetate which on hydrolysis yields the desired 1,15-pentadecanediol.

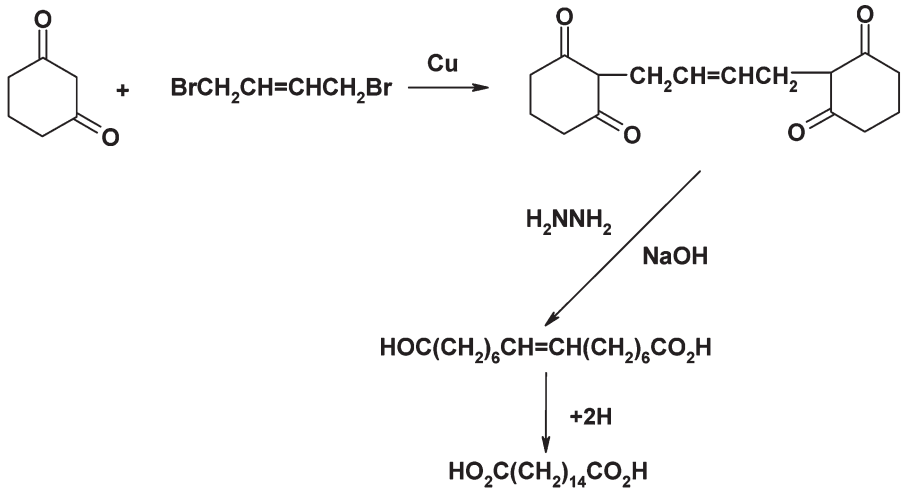

Figure 11. The reaction scheme for the synthesis of 1,16-hexadecanedioic acid.

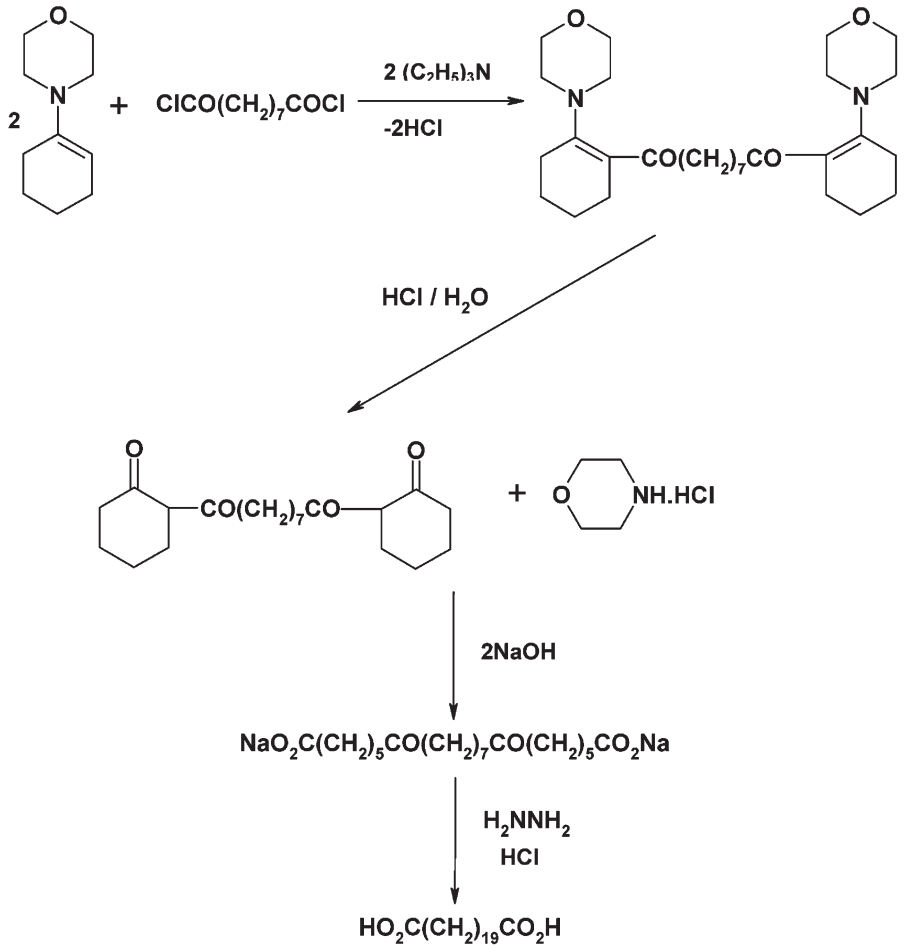

Figure 12. The synthetic strategy used to prepare 1,21-heneicosanedioic acid.

The α,ω-bis(4-cyanobiphenyl-4′-yloxy)alkanes were then assembled from different precursors according to the scheme shown in figure 14. The α,ω-alkanyldioic acids were first reduced to the corresponding α,ω-dihydroxyalkane. Initially these were converted to the α,ω-dibromoalkanes and reacted via a Williamson

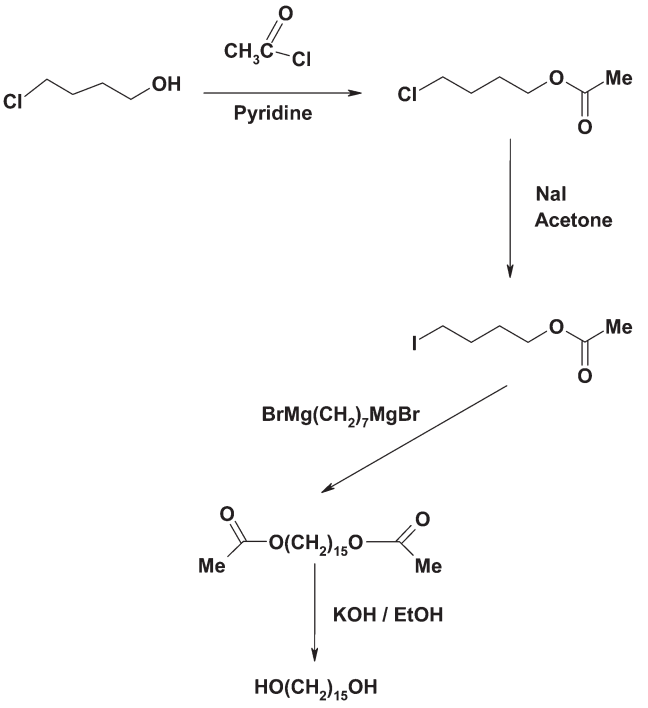

Figure 13. The synthetic route for the preparation of 1,15-pentadecanediol.

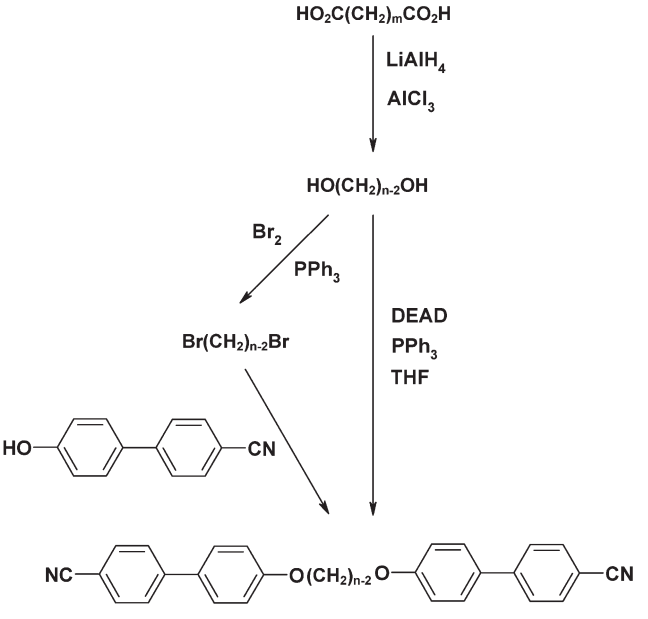

Figure 14. The preparation of the α,ω-bis(4-cyanobiphenyl-4′-yloxy)alkanes starting from the α,ω-alkane diacids or the α,ω-alkane diols.

synthesis to give the α,ω-bis(4-cyanobiphenyl-4′-yloxy) alkanes [39]. However, it was found that this procedure, which involves two steps, was less effective than coupling 4-hydroxy-4′-cyanobiphenyl directly to the α,ω-diol using the Mitsunobu method [43].

The transitional properties of the twelve new liquid crystal dimers with their long spacers were characterized using polarizing optical microscopy and differential scanning calorimetry. The dimers were found to exhibit only nematic phases, as identified by their schlieren textures with both two- and four-point singularities. This is identical to the behaviour of the α,ω-bis(4-cyanobiphenyl-4′-yloxy)alkanes with the shorter spacers (n=3 to 14) [39]. Not all of the new dimers had enantiotropic nematic phases: for even spacers the dimers with 18 or more atoms gave a monotropic nematic as did the odd dimer with a spacer of 23 atoms. However, it was possible with all of these liquid crystal dimers to supercool the isotropic phase below the freezing point and so determine both T_{NI} and $\Delta S/R$, which was our primary aim. Combined with the earlier measurements [39] we now have a continuous homologous series of the α,ω-bis(4-cyanobiphenyl-4′-yloxy) alkanes containing from 3 to 24 atoms. The transitional properties of these nematogens are listed in table 1; they clearly constitute a valuable resource, not only to test

Table 1. The melting points, T_{CrN} or T_{CrI}, nematic–isotropic transition temperatures, T_{NI}, and nematic–isotropic transitional entropies, $\Delta S/R$, of the α,ω-bis(4-cyanobiphenyl-4′-yloxy)alkanes as a function of the spacer length n.

n	T_{CrN}/°C; T_{CrI}/°C	T_{NI}/°C	$\Delta S/R$
3	144	(124)	—
4	205	265	1.77
5	185	(170)	0.54
6	209	250	1.95
7	137	186	0.66
8	187	221	1.98
9	137	181	0.78
10	175	201	2.01
11	133	172	0.94
12	164	184	2.14
13	124	164	1.01
14	149	171	2.08
15	116	152	1.06
16	152	157	2.12
17	109	151	1.13
18	152	(150)	2.19
19	118	145	1.23
20	147	(144)	2.18
21	125	137	1.34
22	135	(131)	2.21
23	130	(126)	1.59
24	136	(128)	2.26

The results for spacer lengths from 3 to 14 are taken from [39]. However, the transitional entropies for n=13 and 14 seemed inconsistent with those of other homologues, the new transitional entropies are listed here. (…) denotes a monotropic nematic–isotropic transition and for these compounds it is the melting point, T_{CrI}, that is given.

theoretical predictions but also for comparison with the behaviour of analogous compounds, as for example the tetrapodes (see § 3).

The nematic–isotropic transition temperatures are plotted as a function of the spacer length in figure 15 together with the melting points for these cyanobiphenyl dimers. The T_{NI} clearly alternate fairly dramatically for short spacers, but just as clearly the alternation is attenuated. Indeed for spacer lengths of 16 or more the alternation has essentially vanished and T_{NI} simply decreases by a small amount with increasing n. Comparison of this behaviour with that predicted by the molecular field theories shown in figure 10 (*a*) is quite striking. It immediately reveals that the predictions based on the discrete model for the conformations of the spacer are in poor agreement with experiment. The alternation in T_{NI} predicted for long spacers is clearly not matched by the experimental results. In marked contrast the variation of T_{NI} given by the continuous model for the conformational states is in remarkable agreement with experiment. The rapid attenuation in the alternation in T_{NI} followed by the continuing slight decrease in the transition temperature with increasing spacer length is exactly what is observed for the homologous series of α,ω-bis(4-cyanobiphenyl-4′-yloxy)alkanes. We should note that the melting points of these dimers shown in figure 15 (*a*) also exhibit an alternation, with the even members having higher melting points than their odd neighbours. The alternation is not attenuated to any significant extent, unlike the behaviour found for T_{NI}. This alternation presumably indicates the ease of packing even dimers with their elongated shape into the crystal lattice in comparison with the bent form for the odd dimers.

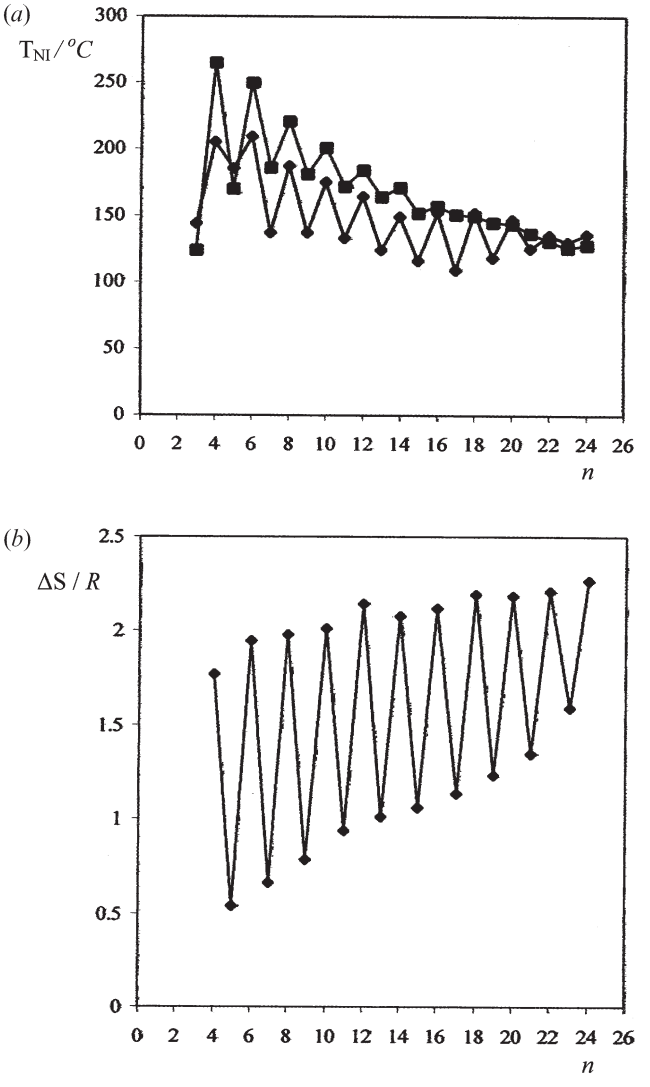

Figure 15. The variation of (*a*) the melting point (◆) and nematic–isotropic transition temperature (■), and (*b*) the entropy change at the nematic–isotropic transition with the spacer length, n, for the α,ω-bis(4-cyanobiphenyl-4′-yloxy) alkanes.

The variation of the entropy change at the nematic–isotropic transition with the spacer length is shown in figure 15 (*b*). The results for the members of this extensive homologous series of cyanobiphenyl dimers exhibit a marked alternation even for the longest spacer, in contrast to the behaviour of the transition temperature, T_{NI}. In addition to the alternation which decreases slightly with increasing n there is also a gradual increase in $\Delta S/R$ with the length of the spacer. As a consequence there is a small reduction in the relative alternation in the transitional entropy as n grows. Comparison of these results with the predictions of $\Delta S/R$ made by the molecular field theories immediately reveals that the discrete model is in poor agreement with experiment, see figure 10 (*b*). The alternation in $\Delta S/R$ for long spacers is clearly too large; in addition the transitional entropy for the even dimers is predicted to increase significantly with spacer length. In contrast the experimental results in figure 15 (*b*) show only a slight increase. As we might have expected the predictions of the continuous model for the conformations are in much better agreement with experiment. The alternation in $\Delta S/R$ is predicted to decrease and the values for the even dimers show only a slight growth with the spacer length; both predictions are in good agreement with experiment. It would seem that in understanding the transitional properties of liquid crystal dimers, and presumably of other liquid crystals composed of highly flexible molecules, the continuous model for the conformational states provides a far better basis than the discrete rotational isomeric state model.

5. Liquid crystal dimers: a constraint molecular dynamics simulation (with P. S. J. Simmonds and D. J. Tildesley)

In the previous section we saw how molecular field theory could help our understanding of the nematic behaviour of liquid crystal dimers with long spacers. For dimers with shorter spacers the reduced molecular complexity means that computer simulation techniques can be used to explore their phase behaviour and the properties of these phases with greater reliability [44]. Here we describe a model for one of the simplest liquid crystal dimers in which two mesogenic groups are linked together with just two methylene groups. The model for the interactions between the mesogenic groups is taken to be the Gay–Berne potential which has been shown to work well for liquid crystal monomers [45]. This generic potential assumes that the molecules are cylindrically symmetric so that their orientations are described by the unit vector, $\hat{\mathbf{u}}$, for the symmetry axis. The pair potential is a single site model in which the energy depends on $\mathbf{r}$, the vector separating the two sites [46]. The dependence resembles a Lennard–Jones 12-6 potential and is written as

$$U(\hat{\mathbf{u}}_i\hat{\mathbf{u}}_j r) = 4\varepsilon(\hat{\mathbf{u}}_i\hat{\mathbf{u}}_j\hat{\mathbf{r}})\left(R^{-12} - R^{-6}\right), \tag{23}$$

where

$$R = \left[r - \sigma(\hat{\mathbf{u}}_i\hat{\mathbf{u}}_j\hat{\mathbf{r}}) + \sigma_0\right]/\sigma_0. \tag{24}$$

Here, the orientation dependence of the contact distance is given by

$$\sigma(\hat{\mathbf{u}}_i\hat{\mathbf{u}}_j\hat{\mathbf{r}}) = \sigma_0\left\{1 - \chi\left[\frac{(\hat{\mathbf{u}}_i\cdot\hat{\mathbf{r}})^2 + (\hat{\mathbf{u}}_j\cdot\hat{\mathbf{r}})^2 - 2\chi(\hat{\mathbf{u}}_i\cdot\hat{\mathbf{r}})(\hat{\mathbf{u}}_j\cdot\hat{\mathbf{r}})(\hat{\mathbf{u}}_i\cdot\hat{\mathbf{u}}_j)}{1-\chi^2(\hat{\mathbf{u}}_i\cdot\hat{\mathbf{u}}_j)^2}\right]\right\}^{-1/2}, \tag{25}$$

where σ_0 is the contact distance for a pair of molecules in the cross configuration. The molecular anisotropy is determined by the parameter χ which is defined by

$$\chi = \left(\kappa^2 - 1\right)/\left(\kappa^2 + 1\right), \tag{26}$$

where κ is the length-to-breadth ratio, σ_e/σ_s. The angular dependence of the well depth is somewhat more involved; it is

$$\varepsilon(\hat{\mathbf{u}}_i\hat{\mathbf{u}}_j\hat{\mathbf{r}}) = \varepsilon_0\varepsilon_1^{\nu}(\hat{\mathbf{u}}_i\hat{\mathbf{u}}_j)\varepsilon_2^{\mu}(\hat{\mathbf{u}}_i\hat{\mathbf{u}}_j\hat{\mathbf{r}}), \tag{27}$$

where ε_0 is the well depth for the molecules, again in a cross configuration. The first angle dependent function is given by

$$\varepsilon_1(\hat{\mathbf{u}}_i\hat{\mathbf{u}}_j) = \left[1 - \chi^2(\hat{\mathbf{u}}_i\cdot\hat{\mathbf{u}}_j)^2\right]^{-1/2} \tag{28}$$

and so is related to the shape anisotropy of the molecule through χ. The second function is

$$\varepsilon_2(\hat{\mathbf{u}}_i\hat{\mathbf{u}}_j\hat{\mathbf{r}}) = 1 - \chi'\left[\frac{(\hat{\mathbf{u}}_i\cdot\hat{\mathbf{r}})^2 + (\hat{\mathbf{u}}_j\cdot\hat{\mathbf{r}})^2 - 2\chi'(\hat{\mathbf{u}}_i\cdot\hat{\mathbf{r}})(\hat{\mathbf{u}}_j\cdot\hat{\mathbf{r}})(\hat{\mathbf{u}}_i\cdot\hat{\mathbf{u}}_j)}{1-\chi'(\hat{\mathbf{u}}_i\cdot\hat{\mathbf{u}}_j)^2}\right] \tag{29}$$

and is clearly analogous to the expression for the contact distance in equation (25). Similarly the parameter χ' is analogous to χ and is defined by

$$\chi' = \left(\kappa'^{1/\mu} - 1\right)/\left(\kappa'^{1/\mu} + 1\right). \tag{30}$$

The quantity κ' provides a measure of the anisotropy in the well depth and is defined by $\varepsilon_s/\varepsilon_e$ where ε_s is the well depth for the side-by-side configuration and ε_e is that for the end-to-end configuration. The exponents ν and μ are adjustable parameters with little direct physical significance. The parameters σ_0 and ε_0 are used to scale distance and energy, respectively, in the simulations. This still leaves four adjustable parameters κ, κ', ν and μ; these are used to denote a particular parameterization of the Gay–Berne potential by GB(κ, κ', ν, μ) [47]. The values of these parameters were initially determined by mapping the potential onto that for a line of four Lennard–Jones atoms [46]; this gave the Gay–Berne mesogen GB(3.0,5.0,2,1) which is known to form isotropic, nematic and crystal phases [48].

The structure of the dimer is sketched in figure 16 (*a*); two Gay–Berne mesogenic groups are linked together at a distance of σ_0 from the molecular centre using a bond $2\sigma_0/3$ in length. The link makes an equilibrium angle θ_0 with the symmetry axes of the two mesogenic groups. The ground state of the dimer is taken to be the *trans* conformation in which the mesogenic groups and the link between them are coplanar. The torsional angle, ϕ, for this conformation is defined to be zero and the torsional energy for larger values is given by the Ryckaert–Bellemans potential

$$U_{\text{tors}}(\phi) = \sum_{n=0}^{5} c_n \cos^n\phi \tag{31}$$

which works well for alkanes [49]; this form is equivalent to that given in equation (6). For such systems the potential contains three minima, one corresponding to the *trans* conformation; the other two equivalent minima are the *gauche*(+) and *gauche*(−) conformations which have a higher energy. In addition we also allow for bond bending by using the harmonic potential suggested by van der Ploeg and Berendsen [50], namely

$$U_{\text{bend}}(\theta) = (k_{\text{bend}}/2)(\theta - \theta_0)^2 \tag{32}$$

where k_{bend} is the force constant for this deformation.

The simulation methodology is taken from the approach used in molecular dynamics simulations of

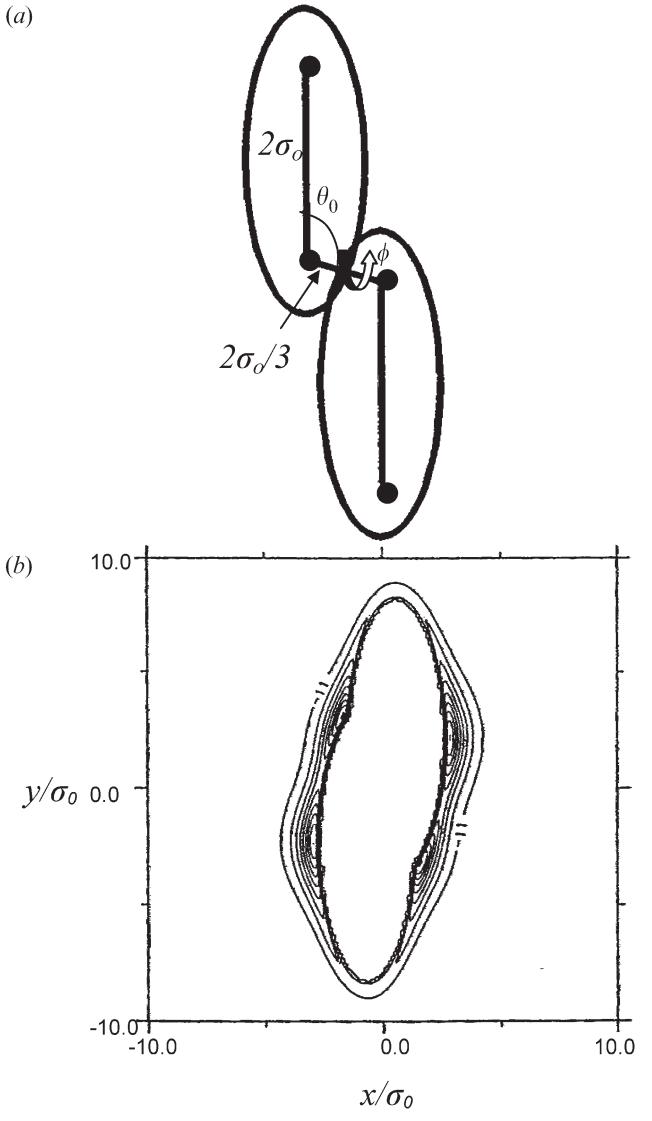

Figure 16. (*a*) The *trans* structure of the flexible liquid crystal dimer formed by linking two Gay–Berne mesogenic groups, showing the location of the four interaction sites and the connection between two of them. (*b*) The potential energy contours for the dimer in its *trans* conformation calculated as another Gay–Berne mesogen, GB(3.0,5.0,2,1), is moved around the dimer with its symmetry axis parallel to those of the mesogenic groups in the dimer. The contours are in ten evenly spaced steps between $-\varepsilon_0$ and zero, corresponding to the contact distance.

polyatomic molecules [51]. Here the equations of motion for the atomic coordinates are solved using the forces on the atoms resulting from the scalar potentials. However, in such simulations it is essential that the bond lengths within the molecule are conserved. This is achieved by the addition of extra terms to the equations of motion, so that in the next time step any changes made to the bond length in the current time step are corrected. In order to be able to implement this methodology for the flexible dimer model that we have designed it is necessary to replace the force and torque which act on the centre of mass and the symmetry axis of a Gay–Berne molecule by forces acting on two centres displaced from the molecular centre of mass. An analogous approach was employed in the first molecular dynamics simulation of a Gay–Berne mesogen [48] and described in [52]. The forces are related to the force, **F**, on the centre of mass and a contribution, $\mathbf{F}_t$, originating from the torque. The sites each have mass $M/2$ and the forces on them are

$$\mathbf{F}_1 = \mathbf{F}/2 + \mathbf{F}_t \tag{33}$$

and

$$\mathbf{F}_2 = \mathbf{F}/2 - \mathbf{F}_t. \tag{34}$$

The contribution from the torque, **T**, is given by

$$2p\hat{\mathbf{e}} \times \mathbf{F}_t = \mathbf{T}, \tag{35}$$

where p is the distance of each site from the centre of mass and $\hat{\mathbf{e}}$ is a unit vector. The y-component of the forces on the two centres coming from the torque is given by

$$F_{ty} = (1/p)\left(T_z\hat{e}_x - T_x\hat{e}_z\right). \tag{36}$$

This can then be used to calculate the x-component

$$F_{tx} = (1/p)\left(p\hat{e}_x F_{ty}/\hat{e}_y - T_z\hat{e}_y\right) \tag{37}$$

which, in turn, is used to obtain

$$F_{tz} = (1/p)\left(p\hat{e}_z F_{tx}/\hat{e}_x - T_y/\hat{e}_x\right). \tag{38}$$

From these results the forces on the two centres can be determined from equations (33) and (34). The forces are then employed in Verlet-like algorithms to evaluate the positions of the four sites in the dimer at the next time, $t+\delta t$. The constraints necessary to maintain constant distances between the sites in a given Gay–Berne mesogenic group, and between the sites that link the two groups together, are applied using the SHAKE algorithm [53]. From the positions of the four sites the new positions and orientations of the Gay–Berne mesogenic groups are recalculated for the next time step and from these the forces on the four sites in the dimers are obtained; see equations (33), (34) and (36) to (38).

We now describe the parameterization of our model dimer. For the two Gay–Berne mesogenic groups we use the original form, namely GB(3.0,5.0,2,1). To show the resulting potential for the dimer we fix it in its *trans* form with θ_0 equal to the tetrahedral angle, 109.47°, and calculate the energy as a single mesogenic molecule, GB(3.0,5.0,2,1), is moved around this with its symmetry

axis parallel to those of the mesogenic groups in the dimer. The energy contours are shown in figure 16 (*b*) and clearly illustrate the Z-shape of the dimer. In addition, deep attractive wells are apparent when the Gay–Berne molecule is adjacent to the mesogenic groups in the dimer, and also near the cusps where the contact contour of one mesogenic group overlaps with that of the other. As we have seen, the Gay–Berne potential contains a parameter ε_0 that is used to scale the energy in the simulation. In contrast, the constants in the Ryckaert–Bellemans potential, as well as the force constant for the bending potential, have absolute values determined from experiment. To convert these to relative values scaled with ε_0 we need an estimate of ε_0; we have obtained this in the following way. First, we note that in simulations of Gay–Berne mesogens which exhibit a nematic–isotropic transition, this invariably occurs when T^* is about 1 [45]. Since the nematic–isotropic transition temperature of typical liquid crystal dimers is of the order of 440 K (see table 1) we set ε_0/k_B to be 440 K. This has been used to give the scaled values of the bending force constant and expansion coefficients listed in table 2. The number of dimer molecules used in the simulation was 108, equivalent to 216 Gay–Berne molecules. This is a relatively small system by current standards but we believe that the behaviour we have observed would not change to any significant extent if a larger system were to be studied. The scaled number density, $\rho* \left(\equiv N\sigma_0^3/V\right)$, used in the microcanonical molecular dynamics simulations was 0.135, which is equal to a number density of 0.27 for the Gay–Berne mesogen typically employed in the study of monomers.

In fact, we have also investigated a system of monomers, GB(3.0,5.0,2,1), using this density to act as a comparison with the behaviour of the dimer. The equilibration run comprised 20k time steps as did the production run. The phases formed by this system were identified from the radial distribution function, $g(r^*)$, and the second rank orientational correlation coefficient, $G_2(r^*)$. This coefficient is defined by

$$G_2(r^*) = \langle P_2\left(\cos\beta_{ij}\right)\rangle_{r^*}, \tag{39}$$

where β_{ij} is the angle between molecules i and j separated by a scaled distance, r^*. In the limit of large separations $G_2(r^*)$ tends to the square of the long range order parameter, $<P_2>$ [54]. The simulations were started at a scaled temperature $T^*(\equiv k_BT/\varepsilon_0)$ of unity, at which point the system was observed to be isotropic, as revealed by $g(r^*)$ and $G_2(r^*)$. The isotropic phase was found to be stable until T^* of 0.4 when the two functions revealed a phase with high orientational and translational order. It has a layered structure with hexagonal packing and, since the molecules were not observed to diffuse within the phase, it is identified as a crystal. The Gay–Berne monomer is then found to form just isotropic and crystal phases at this scaled density, in keeping with other simulations [55].

It is to be expected that linking the two Gay–Berne mesogenic groups will lower the symmetry of the molecule. This should reduce the stability of the crystal phase and so enhance that of the liquid crystal phases. We have investigated three scaled temperatures and report the results for these here. The target temperatures were set as 2.0, 1.10 and 0.90 but during the production run they drifted slightly away from these; the average temperatures for the runs were 2.04 ± 0.05, 1.14 ± 0.03, 0.90 ± 0.02. During the simulations it was found that much longer runs than for the monomer were needed, especially to ensure good conformational equilibration and averaging. The equilibration runs consisted of 40k time steps at T^* of 2.0 and 80k at the two lower temperatures; the production runs all had 120k time steps. The centre of mass of a dimer varies with its conformation and this was calculated from the positions of the four mass sites at each time step. The definition of the orientation requires a particular axis set in the dimer and, because of the changes in the conformation, there is no unique definition for this. We have chosen to identify this as the inertial axis corresponding to the smallest principal component of the inertial tensor; again this was calculated for each dimer at every time step in the production run. Armed with this information we have evaluated the radial distribution function and the orientational correlation coefficient. The results for these are shown for the three temperatures in figure 17. At the highest temperature the radial distribution function is essentially unstructured and tends to its limiting value of unity for the relatively small value, 2.0, of r^*. The lack of any structure near r^* of 1.0 results from the existence of the dimer in different conformational states, which prevents the molecules from approaching close to each other. At the same temperature $G_2(r^*)$ decreases and tends to a limiting value of

Table 2. The scaled expansion coefficients, c_n/ε_0, in the Ryckaert–Bellemans torsional potential and the scaled bending force constant, k/ε_0, used in the simulation of the Gay–Berne dimer.

c_0/ε_0	c_1/ε_0	c_2/ε_0	c_3/ε_0	c_4/ε_0	c_5/ε_0	k_{bend}/ε_0
2.54	3.32	−3.59	−0.84	7.17	−8.61	$142.3\,rad^{-2}$

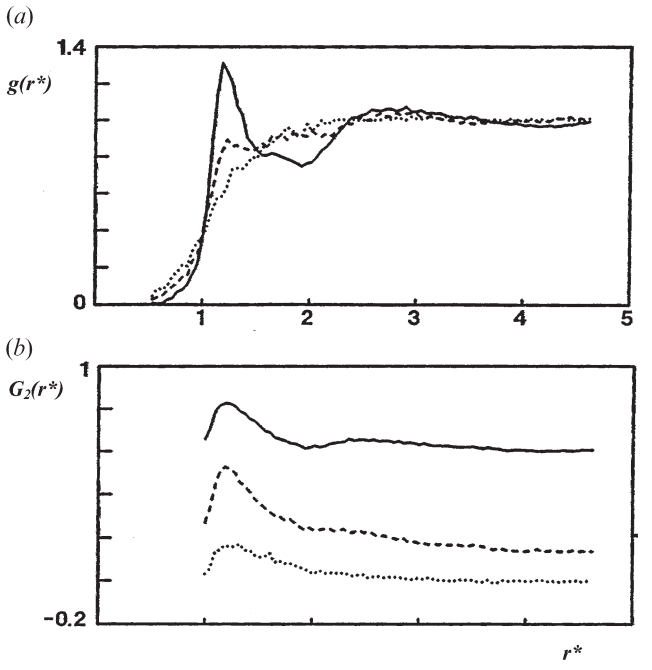

Figure 17. (*a*) The radial distribution function, $g(r^*)$, and (*b*) the second rank orientational correlation coefficient, $G_2(r^*)$, simulated for the Gay–Berne dimer at a scaled number density of 0.135 and at scaled temperatures of 2.04 (···), 1.14 (---) and 0.90 (—).

zero. This value is in accord with the second rank orientational order parameter $<P_2>$ evaluated directly from the Q-tensor introduced by Vieillard–Baron [56]. It is clear, therefore, that at T^* of 2.04 the Gay–Berne dimer exhibits an isotropic phase.

The phase at T^* of 1.14 is different. Here the radial distribution has changed slightly from that in the isotropic phase, see figure 17 (*a*). A weak peak has appeared at r^* of 1.2 which suggests there are more molecules in the *trans* conformation which can approach closer to each other. As we shall see later, the conformational distribution has changed because of the formation of a nematic phase at this lower scaled temperature. The correlation coefficient, $G_2(r^*)$, exhibits a more pronounced peak at r^* of 1.2, showing that neighbouring molecules have a relatively high degree of orientational correlation. This decreases as the separation between the molecules increases but does not decay to zero. The value of $G_2(r^*)$ for a separation of about 4 corresponds to an orientational order parameter of 0.36, which is in good agreement with the value of 0.33 determined from the Q-tensor. The lack of significant structure in $g(r^*)$ together with the non-zero value of $<P_2>$ identifies this as a nematic phase. This assignment is consistent with the more or less uniform density distribution along the director.

At the lowest scaled temperature of 0.90 the structure of the radial distribution function has increased, as we can see in figure 17 (*a*). The first peak, at r^* of 1.2, has grown in intensity, showing a more effective packing of nearest neighbour molecules made possible by an increase in the fraction of dimers in the *trans* conformation. There is also a broad peak at r^* of 2.5 which is suggestive of a layered structure. This view is supported by the density distribution along the director which has a periodic structure, albeit weak, with a scaled periodicity, $d^*(\equiv d/\sigma_0)$ of 2.5. The orientational order in this phase is high as we can see from $G_2(r^*)$ shown in figure 17 (*b*). The intense peak at r^* of 1.2 again reveals the strong correlations between neighbouring molecules. The long range limit of $G_2(r^*)$ gives the orientational order parameter as 0.77, in agreement with its direct evaluation from the Q-tensor. The phase at T^* of 0.90 is identified as a smectic A with a small translational order but a large orientational order.

The assignment of these three phases formed by the Gay–Berne dimer is supported by pictures of their molecular organization taken of configurations from

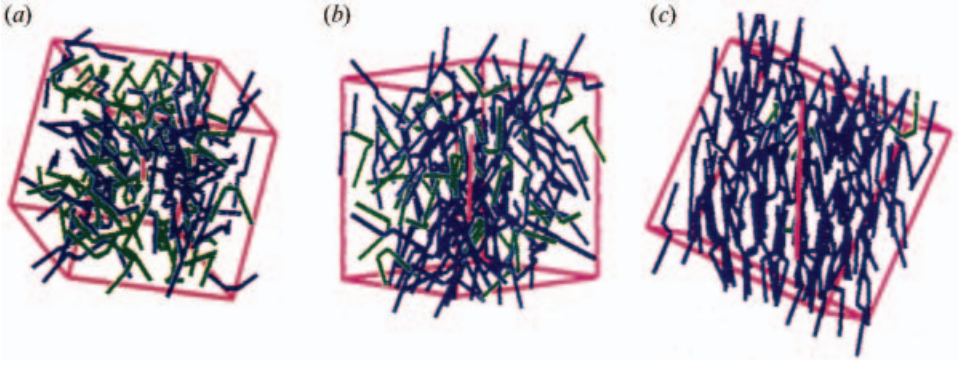

Figure 18. Pictures showing the molecular organization in (*a*) the isotropic phase at T^* of 2.04, (*b*) the nematic phase at T^* of 1.14 and (*c*) the intercalated smectic A phase at T^* of 0.90 for the Gay–Berne dimer. The *trans* conformation ($\phi<60^\circ$) is coloured blue and the *gauche* conformations ($\phi>60^\circ$) are shown as green.

the production runs. The pictures are given in figure 18 and show three features of the system: its orientational order, its translational order and its conformational order. In the isotropic phase at T^* of 2.04 there is no long range translational or orientational order, see figure 18 (*a*). The conformational order is, in principle, hard to judge because the torsional angle can take any value. In practice the dimer tends to adopt conformations approximating to either *trans* or *gauche* forms. These have been colour coded in the image so that all conformers for $\phi<60^\circ$, which includes the *trans* form, are blue while those with $\phi>60^\circ$, which includes the *gauche* form, are green. It is seen that the numbers of *trans* and *gauche* conformers are essentially the same. However, on lowering the scaled temperature to 1.14 into the nematic phase the number of *trans* conformers increases significantly at the expense of the *gauche* form, see figure 18 (*b*). The long range orientational order and translational disorder characteristic of the nematic phase is clearly apparent. Also shown in this and the other pictures is the director orientation; it is indicated by the magenta line, at the centre of the simulation box, whose length is proportional to the orientational order parameter. At the lower scaled temperature of 0.90 the fraction of *gauche* conformers is reduced dramatically to just a few. The *trans* conformers are then able to pack into a weakly layered structure which is clearly apparent in figure 18 (*c*). What is also apparent is the intercalated structure of the smectic A phase (SmA_c); that is, the mesogenic groups of the dimer occupy adjacent layers and do not reside in a single layer. This novel structure explains why the scaled periodicity of the density distribution along the director is just 2.5, which is half the length of the dimer in its *trans* conformation. The stabilization of this intercalated structure may well result from the strong attraction between the mesogenic groups of neighbouring dimers; it is clearly evident from the deep potential wells apparent in the contour plots given in figure 16 (*b*). It is of special interest that the symmetric Gay–Berne dimer forms an intercalated SmA_c phase since such phases are usually exhibited by non-symmetric liquid crystal dimers [57]. The stability of the intercalated phase is interpreted in terms of specific interactions between the different mesogenic groups in adjacent molecules. However, a few symmetric liquid crystal dimers have also been found to form an intercalated smectic phase which is surprising [58]. Our observation that the symmetric model liquid crystal dimer also forms an intercalated smectic A phase provides some support for this.

The pictures in figure 18 clearly show, at a qualitative level, how the probability of finding the dimers in an elongated conformation grows as the orientational order of the phase increases. There is, of course, a contribution to this probability from the reduction in the scaled temperature which accompanies the increase in the orientational order. To quantify the changes in the conformational probability for the Gay–Berne dimers we have calculated the normalized torsional distribution function, $p(\phi)$, which gives the probability of finding the dimer with a torsional angle, ϕ, irrespective of its orientation from the simulations. The results of the distribution function in the three phases are shown in figure 19. At all temperatures the torsional distribution exhibits maxima corresponding to the *trans* ($\phi=0$ rad) and *gauche* ($\phi\approx2.1$ and 4.2 rad) conformations. In the isotropic phase the distribution is slightly higher for the *trans* than for an individual *gauche* conformer. To place these results in context we have calculated the distribution function that would result solely from the torsional potential, namely

$$p(\phi)=Q_{\mathrm{tor}}^{-1}\exp[-U_{\mathrm{tors}}(\phi)/k_{\mathrm{B}}T], \qquad (40)$$

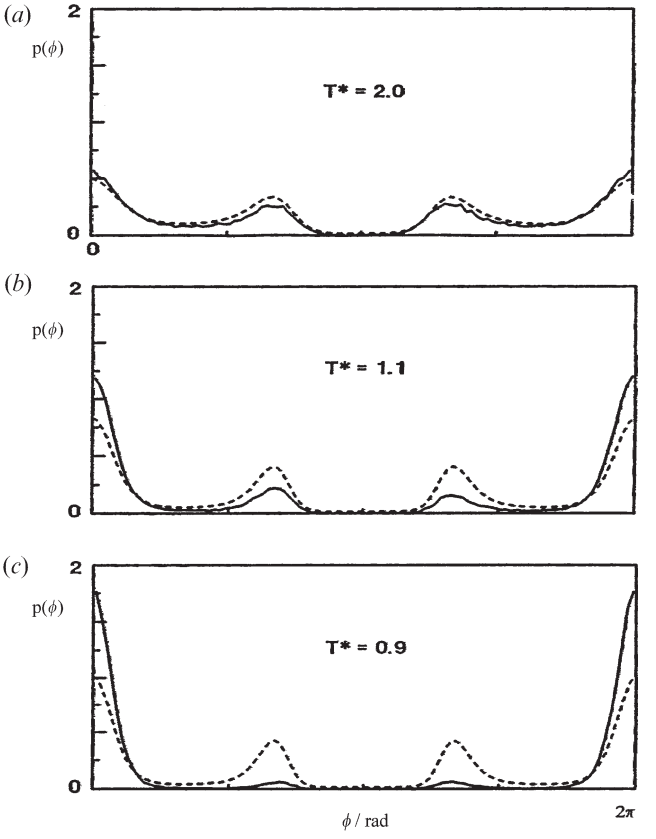

Figure 19. The torsional distribution function, $p(\phi)$, obtained from the simulations of a Gay–Berne dimer in (*a*) the isotropic phase at T^* of 2.04, (*b*) the nematic phase at T^* of 1.14 and (*c*) the intercalated smectic A phase at T^* of 0.90. The dashed lines show the ideal $p(\phi)$ calculated solely from the Ryckaert–Bellemans torsional potential, see equations (31) and (40).

where the conformational partition function is

$$Q_{\rm tor} = \int \exp[-U_{\rm tors}(\phi)/k_{\rm B}T]{\rm d}\phi. \qquad (41)$$

This ideal distribution is what would be expected if the dimer was in the gas phase and if the intramolecular interaction between the Gay–Berne mesogenic groups was negligible, as seems likely. The ideal distribution functions calculated for the three temperatures, 2.04, 1.14 and 0.90, are also shown in figure 19. In the isotropic phase the agreement between the distribution obtained from the simulation and the ideal distribution is very close. This suggests that the distribution is not perturbed in the isotropic phase because the local orientational order is small, see figure 17 (*b*). The torsional distribution in the nematic phase at T^* of 1.14 shows an enhancement and narrowing of the peak associated with the *trans* conformation; in addition the peaks related to the *gauche* conformations decrease in intensity. The ideal distribution function also changes because of the reduction in temperature; thus the probability of the *trans* conformation relative to the *gauche* increases. However, the effect is not nearly as large as that shown by the simulations. Accordingly we can see that the long range orientational order of the nematic phase does have a significant influence on the conformational distribution, enhancing the probability of the *trans* form at the expense of the *gauche*. This novel effect continues in the smectic A_c phase at T^* of 0.90. Here the simulations show, in figure 19 (*c*), that the peak associated with the *trans* form has grown considerably and is almost twice as large as that in the nematic phase. This change is consistent with the increase in $<P_2>$ from 0.33 in the nematic to 0.77 in the SmA_c phase. In contrast, the ideal torsional distribution at T^* of 0.90 differs little from that at 1.14 in the nematic phase. It appears that the high orientational order of the intercalated smectic A phase has a significant effect on the torsional distribution, as theory predicts, see equation (11).

6. Simulations of liquid crystals: the Corner *S*-function potential (with A. Ghahrai and G. Saielli)

The Gay–Berne potential has proved to be an especially valuable model for simulation studies of liquid crystal and their behaviour [45]. This value stems in part from the fact that the potential includes, at a generic level, both attractive and repulsive contributions to the anisotropic interactions. In addition, because this is a single site potential it has a computational simplicity which allows systems containing large numbers of molecules to be studied. As we have seen, equation (23), the potential takes the form

$$U(\hat{\mathbf{u}}_i\hat{\mathbf{u}}_j\mathbf{r}) = 4\varepsilon(\hat{\mathbf{u}}_i\hat{\mathbf{u}}_j\mathbf{r})(R^{-12} - R^{-6}), \qquad (42)$$

where

$$R = [r - \sigma(\hat{\mathbf{u}}_i\hat{\mathbf{u}}_j\mathbf{r}) + \sigma_0]/\sigma_0. \qquad (43)$$

It is similar to a shifted Lennard–Jones 12-6 potential. The shape of a Gay–Berne particle is usually defined by evaluating the contact distance when one molecule is moved around another keeping their symmetry axes parallel. The specific form for this, evaluated from $\sigma(\hat{\mathbf{u}}_i\hat{\mathbf{u}}_j\mathbf{r})$, is ellipsoidal [46]. However, real mesogenic rod-like molecules tend to have a shape that approximates more closely to a spherocylinder [59]. In addition, certain mesogenic molecules deviate from this shape; for example the mesogen formed by linking two 5CB molecules together via a platinum dichloride unit has a structure resembling a spherocylinder with a sphere embedded at its centre [60]. Here we consider how the pair potential for such molecules can be constructed while retaining the essential features of the Gay–Berne model.

One of the earlier approaches to the problem of developing a pair potential for molecules was proposed by Corner [61]. His seminal suggestion was that the distance dependence of the interaction between two molecules with fixed orientations should be given by the Lennard–Jones 12-6 potential

$$U(r) = 4\varepsilon\left[(\sigma/r)^{12} - (\sigma/r)^6\right] \qquad (44)$$

which was known to work well for the scalar interactions between atoms. Its use for molecules requires that the well depth, ε, and the contact distance, σ, depend on the orientations of the two molecules and of the intermolecular vector joining them. He proposed particular functional forms for those dependences relevant for diatomic molecules, which necessarily possess cylindrical symmetry. These expressions are not valid for the larger length-to-breadth ratios of mesogenic molecules. However, the key point to Corner's suggestion is that the pair potential for molecules can be written as a single site potential in which the well-depth and contact distance are orientation dependent. It is apparent, therefore, that the Gay–Berne potential is, in fact, one member of the class of Corner pair potentials. As we have seen, it is not, however, able to model the interaction between spherocylinders and those with an embedded sphere. To achieve this we shall use a novel approach proposed by Zewdie [62] which generalized the functional form first suggested by Corner. Zewdie realized that the parameters in the pair potential could be expanded using a basis of *S*-functions [63]. These are invariant functions of three relative orientations of the cylindrical molecules, with respect to each other

$f_{ij}\left(\equiv\hat{\mathbf{u}}_i\cdot\hat{\mathbf{u}}_j\right)$ and of each molecule with respect to the intermolecular vector, $f_i\left(\equiv\hat{\mathbf{u}}_i\cdot\hat{\mathbf{r}}\right)$ and $f_j\left(\equiv\hat{\mathbf{u}}_j\cdot\hat{\mathbf{r}}\right)$. The parameters in the distance dependent pair potential, which Zewdie took to have the Gay–Berne form, see equation (42), are then expanded as

$$\sigma\left(f_{ij}f_if_j\right)=\sum_{L_1L_2J}\sigma_{L_1L_2J}S_{L_1L_2J}\left(f_{ij}f_if_j\right) \tag{45}$$

and

$$\varepsilon\left(f_{ij}f_if_j\right)=\sum_{L_1L_2J}\varepsilon_{L_1L_2J}S_{L_1L_2J}\left(f_{ij}f_if_j\right). \tag{46}$$

Here L_1 and L_2 are positive integers and J takes values from $|L_1-L_2|$ to L_1+L_2. For linear molecules, non-zero values of the expansion coefficients require that the sum L_1+L_2+J must be positive, and for non-polar molecules L_1, L_2 and J are restricted to even values if $\sigma_{L_1L_2J}$ and $\varepsilon_{L_1L_2J}$ are to be non-zero. The first few S-functions, with even values of L_1, L_2 and J, are given by

$$\begin{aligned}
S_{000}\left(f_{ij}f_if_j\right)&=1\\
S_{202}\left(f_{ij}f_if_j\right)&=\left(3f_i^2-1\right)\Big/2\sqrt{5}\\
S_{022}\left(f_{ij}f_if_j\right)&=\left(3f_j^2-1\right)\Big/2\sqrt{5}\\
S_{220}\left(f_{ij}f_if_j\right)&=\left(3f_{ij}^2-1\right)\Big/2\sqrt{5}\\
S_{222}\left(f_{ij}f_if_j\right)&=\left(2-3f_i^2-3f_j^2-3f_{ij}^2+9f_if_jf_{ij}\right)\Big/\sqrt{70}\\
S_{224}\left(f_{ij}f_if_j\right)&=\left(1+2f_{ij}^2-5f_i^2-5f_j^2-20f_if_jf_{ij}+35f_i^2f_j^2\right)\Big/4\sqrt{70}.
\end{aligned} \tag{47}$$

We can see that when J is zero the S-function depends only on the relative orientation of the two molecules. The expansions are formally correct so that any particular behaviour can be represented by including sufficient terms. Of course, for the potential to be computationally attractive the number of terms in the summations for the contact distance and well depth should be minimized. This has the additional benefit of reducing the number of arbitrary parameters that are employed to define the potential. In practice the number of terms used in the expansions will be a compromise between these factors and the accuracy with which a particular molecular structure is to be represented. In his use of the Corner S-function potential, which we shall refer to as the CornerS potential, to represent the interaction between two spherocylinders with length-to-breadth ratio of 3:1, Zewdie determined the coefficients in the expansion of the contact distance to be those given in table 3 [62].

Here the coefficients are scaled with σ_0, the diameter of the spherocylinder. He also mapped the S-function expansion onto the well-depth, $\varepsilon\left(\hat{\mathbf{u}}_i\hat{\mathbf{u}}_j\hat{\mathbf{r}}\right)$, proposed by Gay and Berne and the expansion coefficients, scaled with ε_0, see equation (27), are given in table 3. We have added a sphere of diameter $1.5\sigma_0$ to the spherocylinder and have obtained the expansion coefficients for this from the contact distances for five configurations namely side-by-side, end-to-end, end-to-side, cross and slipped-parallel. This is one more than the minimum number of configurations needed to extract the coefficients in the expansion for $\sigma(f_{12}f_1f_2)$ restricted to five terms since σ_{202} and σ_{022} must be identical from the equivalence of the molecules. To facilitate comparison with the results obtained for the spherocylinder, the well-depth was taken to have the same expansion coefficients (see table 3). We can visualize the shapes for these two model potentials by plotting the separation when the potential changes from positive to negative for a pair of parallel molecules. The shapes obtained in this way are shown in figure 20 together with that of a Gay–Berne molecule, also with a length-to-breadth ratio of 3:1. The ellipsoidal form of the Gay–Berne molecule is apparent and differs significantly from that of the CornerS spherocylinder. It is noted that this is not an exact spherocylinder presumably because of the restriction on the number of terms in the expansion. The embedded sphere is clearly seen in the contact contour for the third molecule.

The system of particles with embedded spheres was studied using an isobaric–isothermal ensemble (NPT) rather than a canonical ensemble (NVT) [51]. This ensemble was chosen for three reasons. First, because it allows direct contact with experiment where measurements are usually made at constant pressure. Secondly,

Table 3. The scaled expansion coefficients for the contact distance $\sigma^*_{L_1L_2J}$ and for the well depth $\varepsilon^*_{L_1L_2J}$ evaluated for (a) a spherocylinder and (b) a spherocylinder with a central embedded sphere.

	L_1L_2J					
Molecular shape	000	202	022	220	222	224
(a) $\sigma^*_{L_1L_2J}$	1.641	1.436	1.436	−0.599	−0.885	2.323
$\varepsilon^*_{L_1L_2J}$	1.040	−1.404	−1.404	2.199	−0.722	−0.132
(b) $\sigma^*_{L_1L_2J}$	1.834	0.933	0.933	−0.658	−0.678	3.331

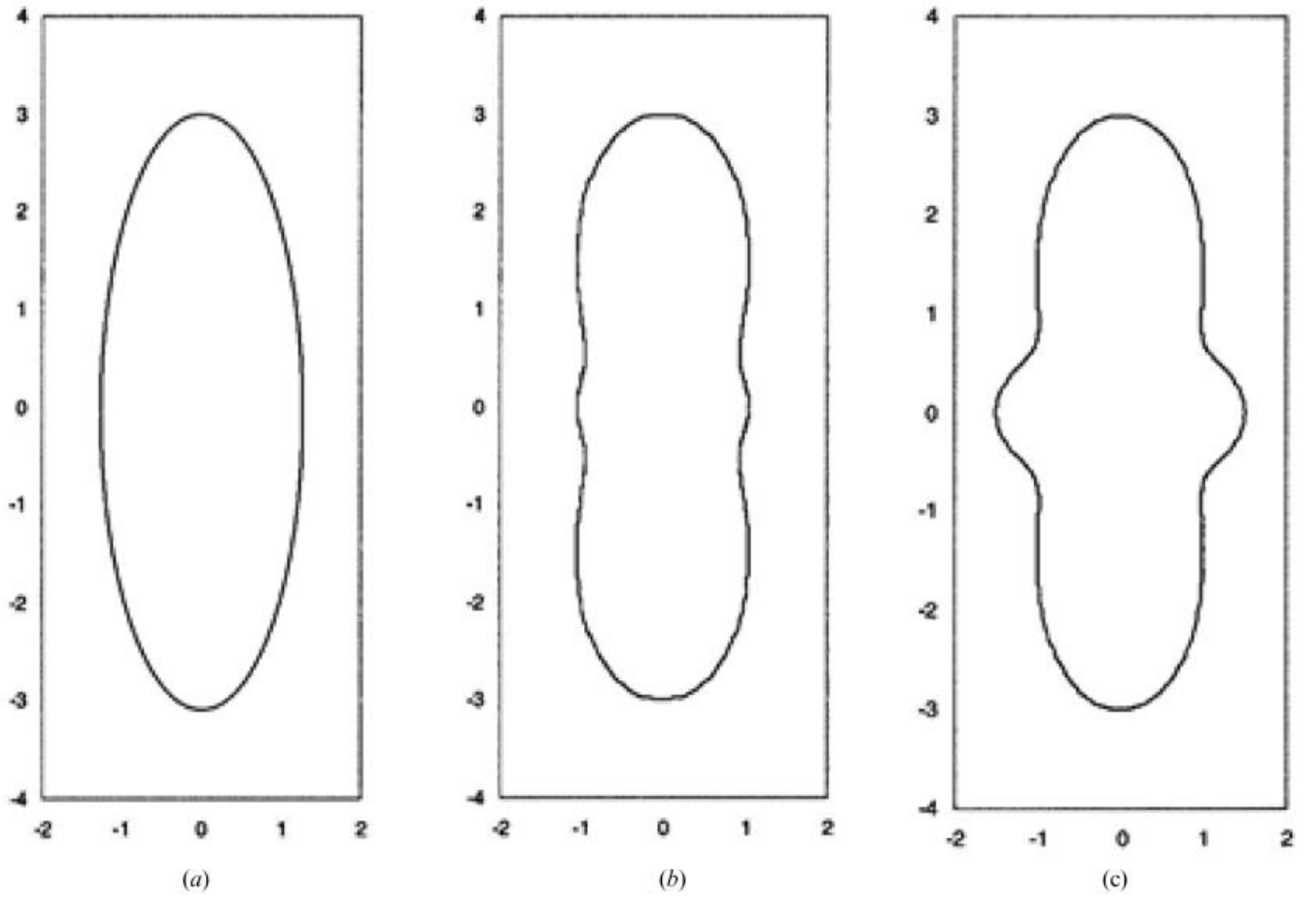

Figure 20. The shapes of three molecules each with a length-to-breadth ratio of 3:1. (*a*) A Gay–Berne molecule, (*b*) a CornerS spherocylinder and (*c*) the same spherocylinder with a central embedded sphere having a diameter of $1.5\sigma_0$.

because at the transition the system will pass directly from one phase to the next, whereas at constant volume the system will pass through a series of coexisting phases. In other words the transition should be sharper at constant pressure than at constant volume. Thirdly, the changes in the box dimensions which occur for the NPT Monte Carlo simulations will allow the molecules in the orthorhombic simulation box to become commensurate with their periodic images when the phases possess long range translational order. In this way the simulation box should not influence the phases that are formed or their structure [52, 64]. The number of molecules used in the simulation was 2000 which is sensibly large. Since Zewdie had used a much smaller system, just 432 molecules and a canonical ensemble, we have performed an NPT simulation for his parameterization of the CornerS potential. This will allow us to compare the behaviour of a system of spherocylinders with that for the system containing an embedded sphere.

We now consider the results of the simulations when the scaled pressure $P^*\left(\equiv P\sigma_0^3/\varepsilon_0\right)$ was set equal to 1.0 and start with the spherocylinder. To locate the phase transitions exhibited by this system we have determined the scaled molecular enthalpy, $H^*(\equiv H/N\varepsilon_0)$, the scaled molecular volume, $V^*\left(\equiv V/N\sigma_0^3\right)$ and the second rank orientational order parameter for the molecular symmetry axis, $<P_2>$, as a function of the scaled temperature, $T^*(\equiv k_BT/\varepsilon_0)$. The results for these quantities are shown in figure 21 for both heating and cooling runs which provide an indication of the hysterisis exhibited at the transitions and so help to distinguish between stable and metastable phases. It is apparent that on cooling from the high temperature phase there is a large jump in both H^* and V^* at T^* of 1.25 ± 0.05, indicating a strong first order transition. In the high temperature phase $<P_2>$ is essentially zero suggesting that this is the isotropic phase and on the other side of the transition $<P_2>$ is about 0.8 which suggests that this is a smectic phase. This tentative assignment is supported by the changes in H^* and V^* at the transition. The jump in the enthalpy gives the transitional entropy, $\Delta S/R$, as 2.01 ± 0.09 which is consistent with that found for a

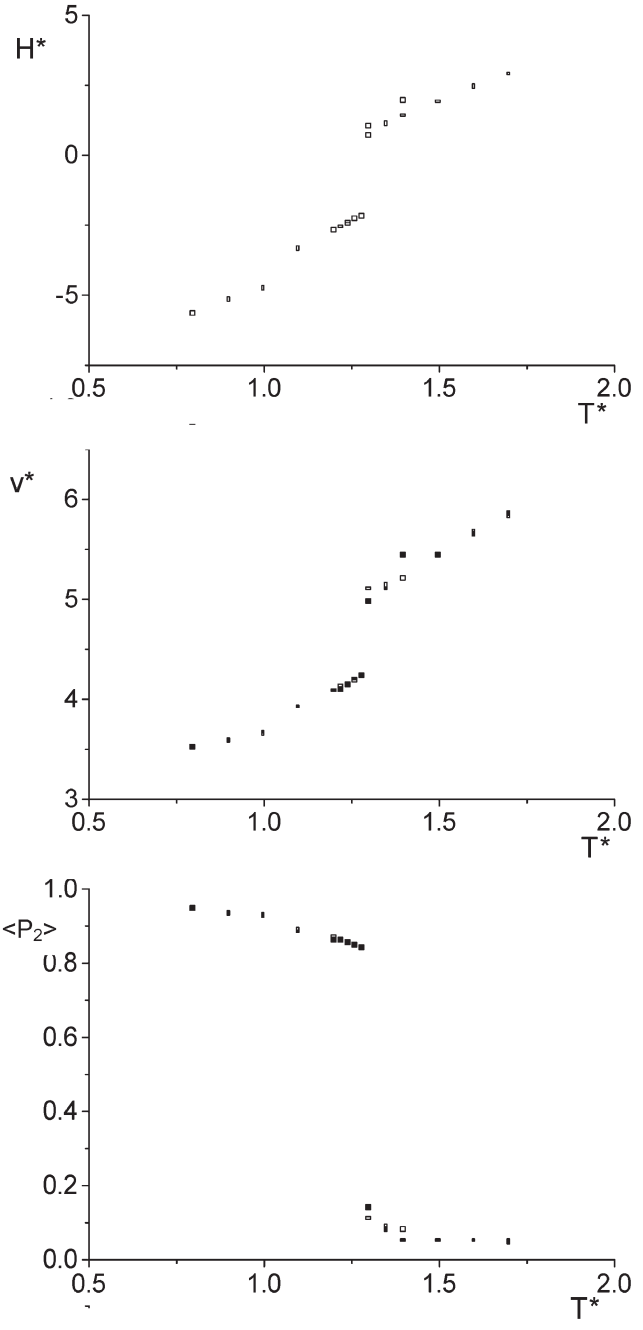

Figure 21. The dependence on the scaled temperature, T^*, of the scaled enthalpy per molecule, H^*, the scaled volume per molecule, V^*, and the second rank orientational order parameter, $\langle P_2 \rangle$. Results obtained on cooling are denoted by ■ and those on heating by □.

SmA–I transition. Similarly the relative change in the volume, $2\left(V_{\mathrm{I}}^* - V_{\mathrm{SmA}}^*\right)/\left(V_{\mathrm{I}}^* + V_{\mathrm{SmA}}^*\right)$, is about 0.15; this is comparable to that found for the SmA–I transition for a Gay–Berne mesogen [47]. On cooling the system further, there is a second first order transition at T^* of 1.05 ± 0.05 although the changes in H^* and V^* are relatively small. In addition, although there is a change in the orientational order parameter it is also small but this is to be expected since the limiting value of $<P_2>$ is unity. Based on this information we are clearly unable to speculate as to the nature of the low temperature phase. The same behaviour is observed on heating, suggesting that the three phases we have observed are stable states for this model potential. There is some hysterisis at the transitions despite the use of runs consisting of 1M cycles and the magnitude of this hysterisis is indicated by the error with which the transition temperatures are quoted.

We now turn to the structural parameters obtained from the simulations in order to identify the three phases formed. One useful way in which to start the identification is to visualize configurations of the particles taken from the production run. The pictures showing such configurations for the three phases are given in figure 22. In the high temperature phase the molecules are randomly oriented and devoid of long range translational order; it is clearly an isotropic phase as we had suggested. The next phase has a layer structure with the molecules tending to be parallel to the layer normal in keeping with the view that this is a smectic A phase. The picture for the lowest temperature phase has a similar structure and on this basis alone it is not possible to distinguish between these phases. However, the radial distribution functions, $g(r^*)$, shown in figure 23 allow us to make this distinction. At a temperature in the isotropic phase the radial distribution is essentially structureless with a single peak at a scaled separation, $r^*(\equiv r/\sigma_0)$, of unity, see figure 23 (*a*). This peak corresponds to spherocylinders that are nearest neighbours, probably with their symmetry axes parallel. The lack of structure confirms the assignment of this as an isotropic phase. The radial distribution for the next phase, figure 23 (*b*), has a strong peak at r^* of unity corresponding to the packing of nearest neighbour spherocylinders that are essentially parallel. There is a weaker peak at r^* of about 2.4 corresponding to next nearest neighbours in the same layer; its broad shape suggests that the translational correlations are not high. The interpretation of the positions of the weaker peaks at larger separations is more difficult because there are contributions to these from spherocylinders in the same and different layers. However, the peaks at r^* of 6.5 and 9.1 could be attributed to molecules in different layers and so reflect the layer structure of the phase.

The radial distribution for the phase at the lowest temperature has a structure quite different from that for the smectic A phase obtained at a higher temperature. Thus the peaks are sharper and so more intense; in addition the observation that they extend to r^* of 10

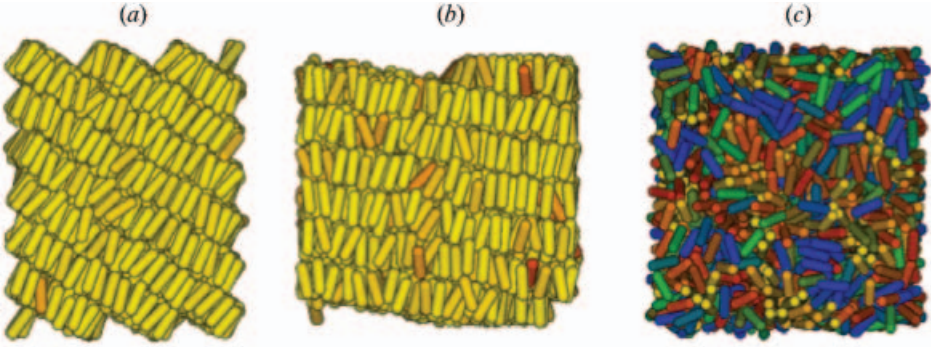

Figure 22. Pictures taken of typical configurations for the three phases, (*a*) crystal/B, (*b*) smectic A and (*c*) isotropic, formed by CornerS spherocylinders. The molecules are colour coded to indicate their orientations.

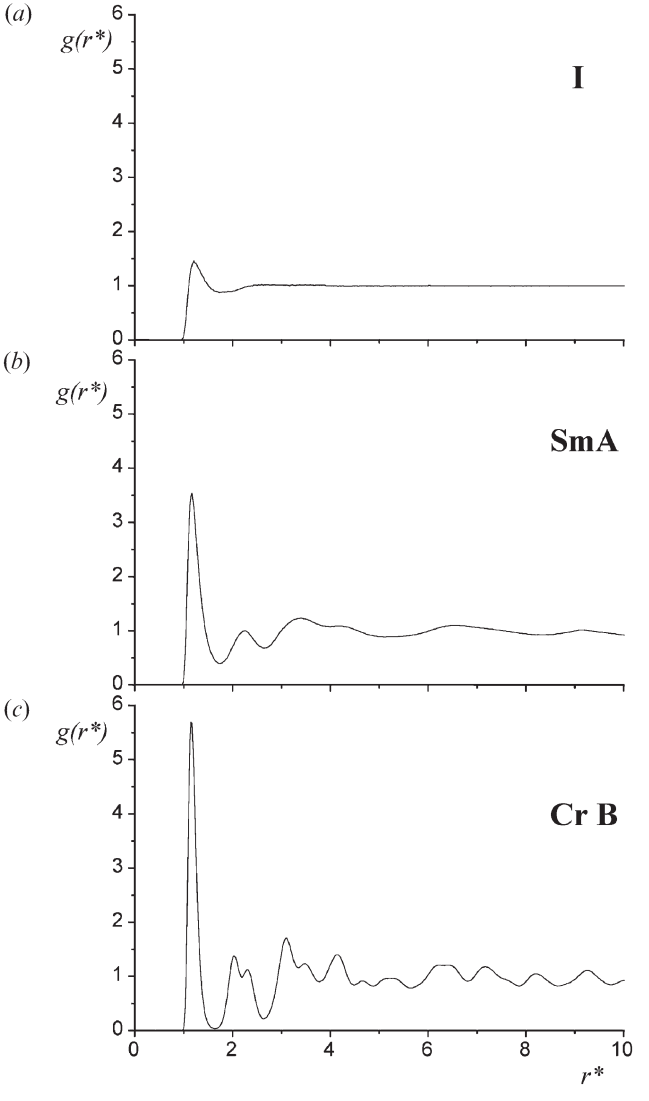

Figure 23. The radial distribution function, $g(r^*)$, for the three phases formed by CornerS spherocylinders calculated at a scaled pressure of 2.0 at T^* of (*a*) 1.8, (*b*) 1.5 and (*c*) 1.1.

shows that the phase has long range translational order. The identity of the phase is hinted at by the observation of two peaks at r^* of about 2 which suggests that the in-plane packing is hexagonal. The phase might be a crystal B phase or simply a crystal. This structure has been explored further by using a range of in-plane distribution functions, $g_{\perp}^{(n)}(r_{\perp}^*)$, which reflect the translational correlations between molecules in the same layer ($n=0$) and for those in neighbouring layers ($n=1$) and in layers that are next nearest neighbours ($n=2$). The form of these $g_{\perp}^{(n)}(r_{\perp}^*)$ functions suggests that the lowest temperature phase is almost certainly a crystal. In addition, they confirm the assignment of the intermediate phase as a smectic A, albeit one with in-plane translational correlations that extend up to about six neighbours which is comparable to that found for the smectic A phase of GB(4.4,20.0,1,1) [47].

It is of relevance to compare the phase behaviour of this CornerS spherocylinder first with that of hard spherocylinders and then with that reported by Zewdie for the same potential. Hard spherocylinders have been well studied as a model for liquid crystals [65]. It is known that in order to observe smectic behaviour the length-to-breadth ratio should exceed 4.1:1, while to form a nematic the ratio should be greater than about 4.7:1. When the length-to-breadth ratio is just 3:1 only crystal and isotropic phases are formed. The observation that the CornerS spherocylinder forms a smectic A phase shows that it must be stabilized by the anisotropic attractive part of the potential which favours the side-by-side arrangement of the spherocylinders. Analogous behaviour is found for the Gay–Berne potential. Here hard ellipsoids do not exhibit smectic phases although the Gay–Berne mesogens certainly form smectic phases [45]. Again these are stabilized by the anisotropic attractive forces. The comparison with the phase behaviour found by Zewdie [62] for the same CornerS potential is more puzzling. He observed the following phases; crystal, smectic B, smectic A, nematic and

isotropic. In marked contrast our simulations show that the model potential leads only to crystal, smectic A and isotropic phases. To ensure that additional phases do not appear at different pressures the simulations were repeated at the higher scaled pressures of 2.0 and 3.0. At both pressures only the same three phases were formed, albeit at different scaled temperatures; the shifts in the scaled transition temperatures are in keeping with the predictions of the Clapeyron equation and the transitional entropy and change in volume obtained from the simulations. In Zewdie's simulations the scaled volume per molecule was kept fixed at a value of 4.35. However, this value is encompassed in our simulations at constant pressure and it is most unlikely that we have missed the phase transitions that he found. The other difference between the two simulations is the system size; we have studied 2 000 molecules whereas he investigated only 432. In addition, the system was studied on heating but not on cooling, so that the stability of the phases formed could not be checked. It seems likely, therefore, that the phases formed by CornerS spherocylinders are not as extensive as reported by Zewdie [62].

We now turn to the phase behaviour for the CornerS spherocylinder with the central embedded sphere and look to see how the sphere modifies the phase behaviour. To locate the phase transitions we have again used the temperature dependence of the scaled molecular enthalpy, the scaled molecular volume and the second rank orientational order parameter. The results for these, obtained at a scaled pressure of 1.0, are given in figure 24. On cooling from high temperature there is a small change in H^* at T^* of 1.75 ± 0.05 and this is matched by an equally small change in V^* at a comparable temperature. In contrast the order parameter shows a large change from a value of less than 0.1 in the high temperature phase to a value of greater than 0.2 but less than 0.5 in the low temperature phase (see figure 24). Clearly we are observing the transition between an isotropic and a liquid crystal phase. The weakness of the transition suggests that the liquid crystal is a nematic. Thus the transitional entropy, $\Delta S/R$, is 0.73 ± 0.05 which is slightly larger than that found for a nematic, while the relative change in volume is 8.7% which is large for a real nematogen but is comparable to the value found for the Gay–Berne mesogen GB(4.4, 20.0, 1, 1) [47]. On lowering the temperature further the system undergoes a second transition at T^* of about 1.25 ± 0.05 at which there are large changes in both H^* and V^*. The changes give $\Delta S/R$ as 3.2 ± 0.05 and the relative change in volume as approximately 63%. These large changes are consistent with the lower temperature phase being a crystal. On heating, the system exhibits a pronounced hysterisis at the low temperature transition in keeping with its strong first order character. In contrast, there appears to be no hysterisis at the high temperature transition, for although this is first order it is weak.

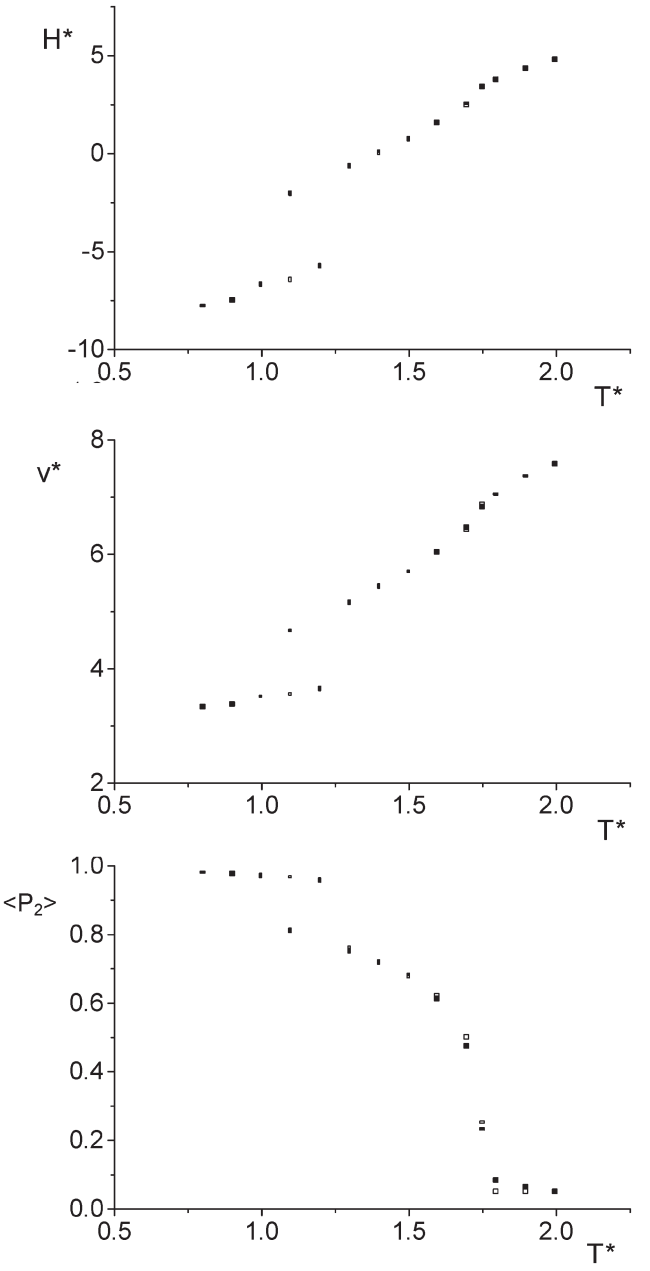

Figure 24. The variation with the scaled temperature, T^*, of the scaled enthalpy per molecule, H^*, the scaled volume per molecule, V^*, and the second rank orientational order parameter, $\langle P_2 \rangle$, determined on cooling (■) and on heating (□) for the CornerS spherocylinder with an embedded sphere.

The tentative assignment of the phases formed by the CornerS potential for a spherocylinder with an embedded sphere as crystal, nematic and isotropic is consistent with the pictures showing the molecular

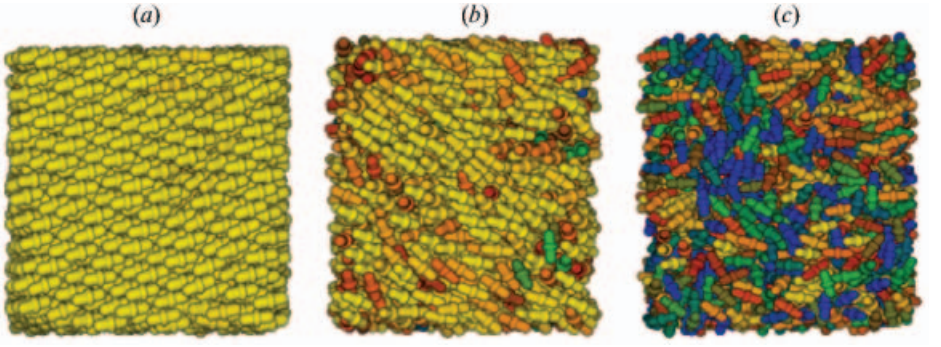

Figure 25. Pictures showing the molecular organization in the three phases (*a*) crystal, (*b*) nematic and (*c*) isotropic, of the CornerS spherocylinder with an embedded sphere. The molecules are colour coded to indicate their orientations.

organization given in figure 25. At the highest temperature both the molecular orientations and positions are devoid of long range order as expected for an isotropic phase. For the next phase the molecular orientations are highly correlated while the centres of mass are essentially randomly arranged. This is typical of a nematic liquid crystal. What is interesting is the local structure where, although the molecules tend to be parallel, the molecular centres are displaced with respect to each other. This slipped-parallel arrangement is consistent with the shape quadrupole, analogous to an electric quadrupole, created in the spherocylinder by the embedded sphere. This slipped-parallel structure becomes long ranged in the lowest temperature phase, which clearly has long range translational as well as orientational order reminiscent of a crystal whose structure is dominated by electric quadrupolar interactions. The phase assignments are further supported by the radial distribution functions shown in figure 26. In the high temperature phase ($T^*=2.60$) $g(r^*)$ contains a single weak broad peak at a scaled distance of about 1.7. This is somewhat larger than the value of 1.5 expected if the spheres of neighbouring molecules were in contact but is consistent with the slipped-parallel local structure. At the lower scaled temperature of 1.8 the radial distribution is essentially the same as for the isotropic phase, which confirms the assignment of this as a nematic phase. In marked contrast the radial distribution for the phase at the lowest scaled temperature of 1.30 is highly structured with relatively sharp peaks. The position of the first of these at r^* of 1.5 is again consistent with a slipped-parallel arrangement for nearest neighbours but would also be in accord with the spheres being in contact. The picture of the molecular arrangement in this phase (see figure 25) allows us to distinguish between these two different structures. In view of the slipped-parallel structure of the phase it is difficult to identify uniquely the pairs of molecules responsible for them. However, because of the structure

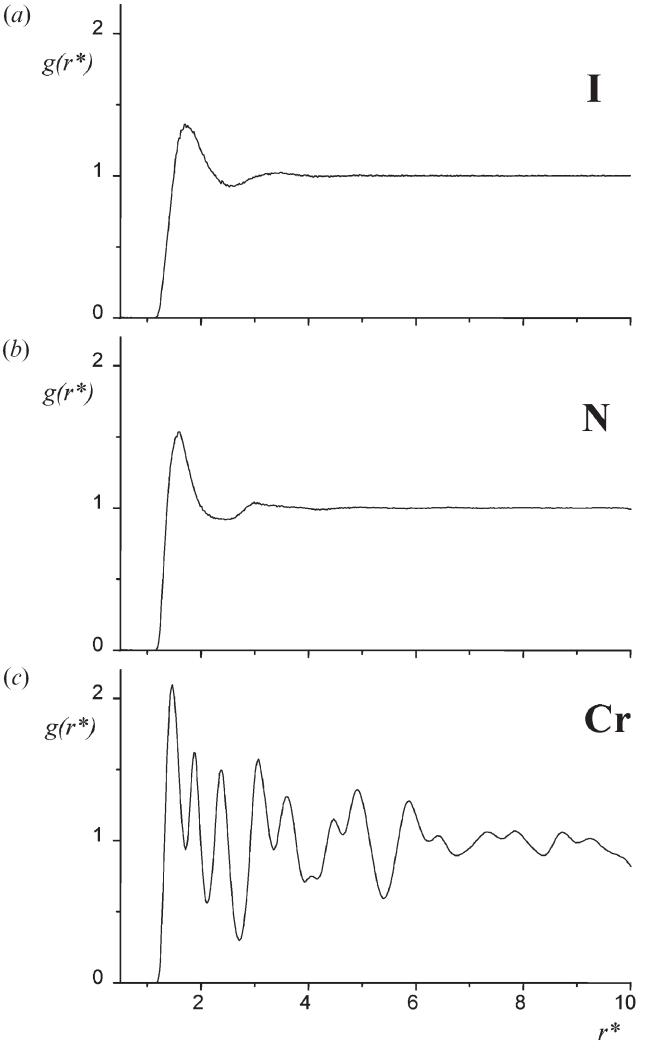

Figure 26. The radial distribution function, $g(r^*)$, for the three phases formed by the CornerS spherocylinder with an embedded sphere at a scaled pressure of 2.0 and scaled temperatures of (*a*) 2.60 (*b*) 1.80 and (*c*) 1.30.

and the long range character of $g(r^*)$ it does seem reasonable to assign this phase as a crystal.

We see, therefore, that the introduction of a central sphere into the spherocylinder has changed dramatically the liquid crystal phases formed. Instead of a smectic A phase as exhibited by the spherocylinders there is now a nematic phase. The system of spherocylinders is able to form a layered structure because of the strong attractive forces stabilizing an arrangement in which the molecules are side-by-side. The same attractive forces are present for the spherocylinders with the embedded spheres but now these are in competition with new packing constraints imposed by the sphere. Two molecules clearly pack more efficiently when parallel but displaced one with respect to the other. This slipped-parallel arrangement resulting from the shape quadrupole clearly destabilizes the smectic A phase and leads to the formation of a nematic phase. As might be expected increasing the diameter of the sphere to $1.75\sigma_0$ is also found to result in the formation of a nematic rather than a smectic A phase. However, it might also be expected that as the diameter of the sphere is reduced a smectic phase and a nematic could both occur. In addition, it seems possible that the tendency to form a slipped-parallel local structure could create a tilted smectic phase rather than a smectic A phase. This conjecture is supported by the observation that the addition of an electric quadrupole to a Gay–Berne potential does indeed result in the formation of a tilted smectic phase [66].

References

[1] D.E. Martire. *The Molecular Physics of Liquid Crystals*, G.R. Luckhurst, G.W. Gray (Eds). Chap. 11, Academic Press, London (1979).

[2] R.L. Humphries, G.R. Luckhurst. *Proc. r. Soc. A*, **352**, 41 (1976); P. Palffy-Muhoray, D.A. Dunmur, W.H. Miller, D.A. Balzarini. *Liquid Crystals and Ordered Fluids*, Vol. 4, p. 615, Plemum Press, New York (1984).

[3] R. Hashim, G.R. Luckhurst, S. Romano. *Proc. r. Soc. A*, **429**, 323 (1990); M.A. Bates. *Phys. Rev. E*, **64**, 051702 (2001).

[4] T. Bellini, M. Caggioni, N.A. Clark, F. Mantegazza, A. Maritan, A. Pelizzola. *Phys. Rev. Lett.*, **91**, 085704 (2003).

[5] D.E. Martire. *Molecular Physics of Liquid Crystals*, G.R. Luckhurst, G.W. Gray (Eds). Chap. 10, Academic Press, London (1979).

[6] G. Rosenblatt. *J. chem. Phys.*, **82**, 2790 (1985).

[7] G.S. Attard, G.R. Luckhurst. *Liq. Cryst.*, **2**, 441 (1987).

[8] G. Brauer. *Handbook of Preparative Inorganic Chemistry* Vol. 2, Academic Press, New York (1965).

[9] T.W. Cheung, S. Fan, G.R. Luckhurst, D.L. Turner. *J. chem. Soc. Faraday Trans.*, **93**, 3099 (1997).

[10] J.W. Emsley, G.R. Luckhurst, C.P. Stockley. *Proc. r. Soc. A*, **381**, 117 (1982).

[11] J.W. Emsley. NMR in Oriented Phases, Tropea, Italy. 29th September–2nd October, 2005.

[12] S. Marcelja. *Biochim. Biophys. Acta*, **367**, 165 (1974).

[13] D.J. Photinos, E.T. Samulski, H. Toriumi. *J. phys. Chem.*, **94**, 4688 (1990).

[14] C.A. Veracini. *Nuclear Magnetic Resonance of Liquid Crystals*, J.W. Emsley (Ed.). Chap. 5, Reidel, Dordrecht (1985).

[15] C.J.R. Counsell, J.W. Emsley, N.J. Heaton, G.R. Luckhurst. *Mol. Phys.*, **54**, 847 (1985).

[16] H. Reuter, R. Pawlak. *Z. Kristallogr.*, **231**, 147 (1998); W.H. Pearson, A.C. Lindbeck, J.W. Kampf. *J.Am.chem. Soc.*, **115**, 2622 (1993).

[17] I. Haller. *Prog. solid-state Chem.*, **10**, 103 (1975).

[18] C.T. Imrie. *Physical Properties of Liquid Crystals: Nematics*, D.A. Dunmur, A. Fukuda, G.R. Luckhurst (Eds). Chap. 1.3, INSPEC, London (2001).

[19] S.A. Ponomarenko, E.A. Rebrov, A. Yu Bobrovsky, N.I. Boiko, A.M. Muzafarov, V.P. Shibaev. *Liq. Cryst.*, **21**, 1 (1996).

[20] R. Elsäßer, G.H. Mehl, J.W. Goodby, M. Veith. *Angew. Chem. int. Ed.*, **40**, 2688 (2001).

[21] R. Eidenschink, F.H. Kreuzer, W.H. de Jeu. *Liq. Cryst.*, **8**, 879 (1990).

[22] J.W. Goodby, G.H. Mehl, I.M. Saez, R.P. Tuffin, G. Mackenzie, R. Auzely-Velty, T. Benvegnu, D. Plusquellec. *Chem. Commun.*, 2057 (1998).

[23] R. Elsäßer, J.W. Goodby, G.H. Mehl, D. Rodriguez Martin, R.M. Richardson, D.J. Photinos, M. Veith. *Mol. Cryst. liq. Cryst.*, **402**, 237 (2003).

[24] K. Merkel, A. Kocot, J.K. Vij, R. Korlacki, G.H. Mehl, T. Meyer. *Phys. Rev. Lett.*, **93**, 237801 (2004); J.L. Figueirinhas, C. Cruz, D. Filip, G. Feio, A.C. Ribeiro, Y. Frère, T. Meyer, G.H. Mehl. *Phys. Rev. Lett.*, **94**, 107802 (2005).

[25] P.J. Flory. *Statistical Physics of Chain Molecules*. Wiley, New York (1969).

[26] S. Marcelja. *J. chem. Phys.*, **60**, 3599 (1974); A. Ferrarini, G.R. Luckhurst, P.L. Nordio, S.J. Roskilly. *J. chem. Phys.*, **100**, 1460 (1994); G.R. Luckhurst. *Mol. Phys.*, **82**, 1063 (1994).

[27] A. Ferrarini, G.R. Luckhurst, P.L. Nordio. *Mol. Phys.*, **85**, 131 (1995).

[28] J.W. Emsley, G.R. Luckhurst. *Mol. Phys.*, **41**, 19 (1980).

[29] J.P. Ryckaert, A. Bellemans. *Chem. Phys. Lett.*, **30**, 123 (1975).

[30] G.R. Luckhurst, C. Zannoni, P.L. Nordio, U. Segre. *Mol. Phys.*, **30**, 1345 (1975).

[31] G.M. Torrie, J.P. Valleau. *J. comput. Phys.*, **23**, 187 (1977).

[32] W.L. Jorgensen. *BOSS, Version 3.8*. Yale University, New Haven CT (1997).

[33] See, for example, G.R. Luckhurst. *The Molecular Physics of Liquid Crystals*, G.R. Luckhurst, G.W. Gray (Eds). Chap. 4, Academic Press, London (1979).

[34] A. Kloczkowski, G.R. Luckhurst. *Liq. Cryst.*, **3**, 95 (1988).

[35] J.W. Emsley, G.R. Luckhurst, G.N. Shilstone. *Mol. Phys.*, **53**, 1023 (1984).

[36] A. Ferrarini, G.R. Luckhurst, P.L. Nordio, S.J. Roskilly. *Chem. Phys. Lett.*, **214**, 409 (1993).

[37] D. Vorländer. *Z. phys. Chem.*, **126**, 449 (1927).

[38] A.C. Griffin, T.R. Britt. *J. Am. chem. Soc.*, **103**, 4957 (1981).

[39] J.W. Emsley, G.R. Luckhurst, G.N. Shilstone, I. Sage. *Mol. Cryst. liq. Cryst. Lett.*, **102**, 223 (1984).

[40] H. Stetter, W. Dierichs. *Chem. Berich.*, **85**, 1061 (1952).

[41] S. Hünig, E. Lücke, W. Brenninger. *Org. Synth.*, **43**, 34 (1963).
[42] D.E. Bergbreiter, G.M. Whitesides. *J. org. Chem.*, **40**, 779 (1975).
[43] O. Mitsunobu. *Synthesis*, 1 (1981).
[44] M.R. Wilson. *J. chem. Phys.*, **107**, 8654 (1997).
[45] M.A. Bates, G.R. Luckhurst. *Struct. Bond.*, **94**, 65 (1998).
[46] J.G. Gay, B.J. Berne. *J. chem. Phys.*, **74**, 3316 (1981).
[47] M.A. Bates, G.R. Luckhurst. *J. chem. Phys.*, **110**, 7087 (1999).
[48] D.J. Adams, G.R. Luckhurst, R.W. Phippen. *Mol. Phys.*, **61**, 1575 (1987).
[49] J.P. Ryckaert, A. Bellemans. *Farad. Disc. chem. Soc.*, **66**, 95 (1978).
[50] P. van der Ploeg, H.J.C. Berendsen. *Mol. Phys.*, **49**, 223 (1983).
[51] M.P. Allen, D.J. Tildesley. *Computer Simulation of Liquids*, Chap. 3, Oxford University Press (1989).
[52] G.R. Luckhurst, R.A. Stephens, R.W. Phippen. *Liq. Cryst.*, **8**, 451 (1990).
[53] J.P. Ryckaert, G. Ciccotti, H.J.C. Berendsen. *J. comput. Phys.*, **23**, 327 (1977).
[54] C. Zannoni. *The Molecular Physics of Liquid Crystals*, G.R. Luckhurst, G.W. Gray (Eds). Chap. 9, Academic Press, London (1979).
[55] E. de Miguel, L.F. Rull, M.K. Chalam, K.E. Gubbins. *Mol. Phys.*, **71**, 1223 (1990); E. de Miguel, L.F. Rull, M.K. Chalam, K.E. Gubbins, F. van Swol. *Mol. Phys.*, **72**, 593 (1991).
[56] J. Vieillard-Baron. *Mol. Phys.*, **28**, 809 (1974).
[57] J.L. Hogan, C.T. Imrie, G.R. Luckhurst. *Liq. Cryst.*, **3**, 645 (1988); G.S. Attard, R.W. Date, C.T. Imrie, G.R. Luckhurst, S.J. Roskilly, J.M. Seddon, L. Taylor. *Liq. Cryst.*, **16**, 529 (1994).
[58] J. Watanabe, H. Komura, T. Niori. *Liq. Cryst.*, **13**, 455 (1993).
[59] G.R. Luckhurst, P.S.J. Simmonds. *Mol. Phys.*, **80**, 233 (1993).
[60] B. Donnio, D.W. Bruce. *J. chem. Soc. Dalton Trans.*, 2745 (1997).
[61] J. Corner. *Proc. r. Soc. A*, **192**, 275 (1948).
[62] H.B. Zewdie. *J. chem. Phys.*, **108**, 2117 (1998).
[63] L. Blum, A.J. Torruella. *J. chem. Phys.*, **51**, 303 (1972); see also A.J. Stone. *The Molecular Physics of Liquid Crystals*, G.R. Luckhurst, G.W. Gray (Eds.) Chap. 2, Academic Press, London (1979).
[64] R. Hashim, G.R. Luckhurst, S. Romano. *J. chem. Soc. Faraday Trans.*, **91**, 3177 (1995).
[65] P. Bolhuis, D. Frenkel. *J. chem. Phys.*, **106**, 666 (1997).
[66] I.M. Withers. *J. chem. Phys.*, **119**, 10209 (2003).